A crystal engineering approach for rational design of curcumin crystals for Pickering stabilization of emulsions

Food Research International 194 (2024) 114871

Contents lists available at ScienceDirect

Food Research International

journal homepage: www.elsevier.com/locate/foodres

A crystal engineering approach for rational design of curcumin crystals for Pickering stabilization of emulsions

Giulia Del Duca [a], Emmanuele Parisi [a], Fiora Artusio [a], Eleonora Calì [a], Silvia Fraterrigo Garofalo [a], Chiara Rosso [b], Valentina Cauda [a], Michele R. Chierotti [b], Elena Simone [a,*]

[a] Department of Applied Science and Technology (DISAT), Politecnico di Torino, 10129 Torino, Italy
[b] Department of Chemistry and NIS Centre, University of Torino, V. Giuria 7, 10125 Torino, Italy

ARTICLE INFO

Keywords:
Crystal engineering
Curcumin
Pickering
Anti-solvent crystallization

ABSTRACT

Emulsions stabilized via Pickering particles are becoming more and more popular due to their high stability and biocompatibility. Hence, developing new ways to produce effective Pickering particles is essential. In this work, we present a crystal engineering approach to obtain precise control over particle properties such as size, shape, and crystal structure, which may affect wettability and surface chemistry. A highly reproducible synthesis method via anti-solvent crystallization was developed to produce sub-micron sized curcumin crystals of the metastable form III, to be used as Pickering stabilizers. The produced crystals presented a clear hydrophobic nature, which was demonstrated by their preference to stabilize water-in-oil (W/O) emulsions. A comprehensive experimental and computational characterization of curcumin crystals was performed to rationalize their hydrophobic nature. Analytical techniques including Raman spectroscopy, powder X-ray diffraction (PXRD), Solid-State Nuclear Magnetic Resonance (SSNMR), scanning electron microscopy (SEM), Differential Scanning Calorimetry (DSC), confocal fluorescence microscopy and contact angle measurements were used to characterize curcumin particles in terms of shape, size and interfacial activity. The attachment energy model was instead applied to study relevant surface features of curcumin crystals, such as topology and facet-specific surface chemistry. This work contributes to the understanding of the effect of crystal properties on the mechanism of Pickering stabilization, and paves the way for the formulation of innovative products in fields ranging from pharmaceuticals to food science.

1. Introduction

Emulsions are widely used in the food and pharmaceutical industries for encapsulation, controlled release, and delivery of active compounds (Chen et al., 2020; Frelichowska et al., 2009; Tan & McClements, 2021; Tang et al., 2015).

In recent years, there has been a growing interest in Pickering systems (Dickinson, 2010; Ewens et al., 2021; Metilli et al., 2022; Yang et al., 2017), a specific type of emulsion stabilized by solid particles, which irreversibly adsorb at the interface between two immiscible phases (Chevalier & Bolzinger, 2013). The use of solid particles to stabilize interfaces offers more appealing properties compared to synthetic surfactants (Binks, 2002); in fact, Pickering systems present lower tendency to coalescence of the dispersed phase, higher mechanical resistance and enhanced thermodynamic stability (Albert et al., 2019; Aveyard et al., 2003). Additionally, food-grade particles derived from natural sources can be used as stabilizers for food, pharmaceutical and agrochemical applications. Compared to traditional stabilizers food-grade, natural particles are more sustainable, less toxic, more biocompatible and are associated to less negative side effects like irritation and allergies (Tang et al., 2015).

The formation mechanism, thermodynamic stability, and functionality of Pickering emulsions are influenced by many factors, including particle wettability, size, and morphology (e.g., aspect ratio) distributions (Pugh, 2016; Wu & Ma, 2016; Xia et al., 2021). Therefore, a correct design of crystalline particles and the related production processes is crucial to obtain the desired multiphase system performance.

The type of emulsion stabilized by Pickering particles, whether oil-in-water (O/W) or water-in-oil (W/O), is influenced by the surface nature of Pickering particles. This is often described by the three-phase contact angle (θ) formed between the solid particle and the oil/water interface. When the angle formed on the water side (θ_w) is less than 90°,

* Corresponding author.
E-mail address: elena.simone@polito.it (E. Simone).

https://doi.org/10.1016/j.foodres.2024.114871
Received 11 April 2024; Received in revised form 10 July 2024; Accepted 5 August 2024
Available online 6 August 2024

particles are more suitable for the stabilization of O/W emulsions. On the contrary, when this contact angle exceeds 90°, the formation of W/O emulsion is more favoured (Binks & Lumsdon, 2000).

The size distribution of Pickering particles also influences directly the average size of emulsion droplets formed during emulsification. Typically, Pickering particles are at least one order of magnitude smaller than the average size of emulsion droplets (Xia et al., 2021). Particle morphology (e.g., aspect ratio) was also found to have an effect on Pickering stabilization; particles characterized by a high value of aspect ratio, such as ellipsoids, fibres and rods, were found to better stabilize emulsion droplets compared to more spherical shapes (Jafari et al., 2020).

A variety of plant-derived particles, such as polysaccharides (e.g., cellulose, starch, chitosan), proteins, and polyphenol crystals (Luo et al., 2011), can be utilized to stabilize emulsions. Crystalline polyphenols, including curcumin, are particularly attractive due to their edibility, cost-effectiveness, and health benefits (Xiao et al., 2021). Curcumin is one of the most recently studied compounds (Nelson et al., 2017), which also exhibits surface activity (Aditya et al., 2017; Sarkar & Dickinson, 2020; Zembyla et al., 2018, 2019, 2020). Furthermore, curcumin has a high tendency to arrange in different crystal structures, such as polymorphs or co-crystals (Sanphui & Bolla, 2018). Polymorphs and co-crystals of the same compound can present different bulk properties such as solubility, thermodynamic stability, and dissolution rate; but also different surface features (i.e., roughness and chemical nature), which can be rationally linked with crystal structure properties (Klitou et al., 2022, 2023; Prandini et al., 2024; Preston et al., 2024).

In this work, a crystal engineering approach was used to develop a robust methodology for the synthesis of sub-micron curcumin particles suitable for Pickering stabilization. In particular, crystal engineering tools such as molecular modelling (e.g., Particle Informatics) and multi-technique particle characterization techniques (e.g., SEM, DSC, XRD) were used to relate crystal structure with important Pickering properties such as roughness and surface chemistry (Desiraju, 2013).

Curcumin crystals were obtained by anti-solvent crystallization, a technique that offers better control over crystal size and shape distribution compared to classical top-down methodologies such as micronization (e.g., jet or ball milling). Additionally, anti-solvent crystallization prevents the formation of amorphous, unstable particles, (Thorat & Dalvi, 2012) and favours the growth of crystals with narrow size and shape distributions. On the other hand, anti-solvent crystallization processes make use of organic solvents, which usually needs to be separated from the anti-solvent (e.g., via distillation) after particles have formed. Additionally, this particle production technique requires further unit operations such as filtration or centrifugation to separate solid particles from the mother liquor.

Following another typical crystal engineering approach (Simone & Nagy, 2015; Simone et al., 2015), we performed a systematic investigation of the relationship between crystallization conditions (e.g., stirring rate, ratio solvent to anti-solvent, volume, and concentration) and curcumin crystal shape (aspect ratio), size and polymorphism using Design of Experiment (DoE). Finally, interfacial properties of curcumin crystals were studied with contact angle measurements, emulsification experiments, and confocal fluorescence microscopy. This work highlights a clear relationship between crystal properties of curcumin particles (size, shape, polymorphic form) and their ability to act as Pickering stabilizer, showing that a crystal engineering approach can be effective in the design of Pickering particles and the processes necessary to produce them.

2. Materials and methods

Curcumin from turmeric rhizome (98 wt% total curcuminoid content, >78 wt% curcumin) was obtained from Thermo Fisher Scientific. Ethanol (99.98 %) was purchased from Sigma-Aldrich. Medium-chain triglycerides (MCT) oils (Nature Aid) was purchased from a local store. Water purified by treatment with a Milli-Q apparatus was used for all the experiments. The curcuminoid mixture was used without further purification and will be referred to as "raw curcumin" from now on in this paper. The presence of structurally related impurities (Fig. 1) is not a limitation for the purpose of this work. Curcumin molecules in the crystal lattice mainly interact via hydrogen bonding interactions that do not involve the methoxy groups; these are not even involved in any significant intramolecular interaction that can be responsible for molecular torsion (Heffernan et al., 2018). Thus, the presence of a high concentration of demethoxycurcumin incorporated in the crystal structure does not greatly affect the properties of the powder.

2.1. Solubility measurement in ethanol

The solubility of curcumin as purchased (form I) in ethanol was determined using the Crystal 16 apparatus (Technobis). Curcumin was previously gently ground in a mortar using an agate pestle, then weighed and dispersed in ethanol in a 1.5 mL vial. 12 slurries at different concentrations were prepared. Bottom stirring at a fixed speed of 780 rpm was used to keep the particles well dispersed. The samples underwent three consecutive dissolution and recrystallization cycles, by changing temperature from 0 °C to 70 °C, with a heating rate of 0.3 °C/min and a cooling rate of −0.3 °C/min.

2.2. Solubility measurement in ethanol–water mixtures

Raw curcumin in ethanol–water mixtures in different ratios was quantified with a high-performance liquid chromatography (HPLC) system (Shimadzu 20A Nexera). A Kinetex core shell C18 column (5 μm, 150 × 4.6 mm) by Phenomenex and a photo diode array detector were employed to quantify the solute dissolved in the mixtures. Curcumin and solvents absorbance was previously evaluated; 425 nm wavelength was selected. The mobile phase used consisted of acetonitrile and 0.1 % formic acid at a ratio of 50/50 (v/v). The analytes were eluted using an isocratic elution method with a flow rate maintained at 0.8 mL/min, and the column oven temperature fixed at 40 °C. The injection volume was set at 10 μL (Peram et al., 2017). The calibration curve was obtained starting from a series of standard solutions of raw curcumin in ethanol with varying concentrations from 0.1 μg/mL to 100.0 μg/mL, obtained by serial dilutions from the 100.0 μg/mL ethanolic stock solution. A total of nine points were collected in duplicate. The quantification of curcumin dissolved in ethanol–water mixtures with increasing water content (ratio ranging from 1:2.5 to 1:20 w/w) was determined by interpolation from the calibration curve. The analyte composition of the solvent had no significant effect on the precision of the calibration method. The analyte samples were prepared stirring for 15 min an excess of raw curcumin in the ethanol–water mixtures. The excess precipitate was allowed to settle, and the dispersions were filtered using a 22 μm syringe filter. The resulting solutions were then placed in HPLC vials for quantification. The measurements were conducted in triplicate.

2.3. Anti-solvent crystallization experiments

Anti-solvent crystallization experiments were designed considering different operating conditions, namely the concentration of curcumin in the ethanolic solution, the ethanol–water ratio, the final volume of the crystallization solution, and the speed of stirring during the anti-solvent addition. A Design of Experiment (DoE) approach was used to plan a set of experiments varying these four different factors. Five different levels for each factor were considered (Supporting Info Table S1). The experimental matrix was generated using the default *ccdesign* function in MATLAB R2021a. A statistical analysis of the effect of these different experimental factors (and their combinations) on particle average size and aspect ratio was conducted using the Chemometric Agile Tool (CAT) 3.1.2 software, freely available from https://www.gruppochemiometria.it/f following the approach shown by (Leardi, 2009).

Table 1
List of the experiments performed. DoE approach was used. The four factors and the five levels were first combined in a full factorial design, for a total amount of 625 experimental points. ccdesign function was then applied to select the experiments from the experimental domain.

Experiment #	Concentration (mg/g)	EtOH/ Water Ratio	Water volume (ml)	Speed mixing (rpm)
Exp 1	7.25	01:12.5	445	14,900
Exp 2	7.25	01:12.5	445	18,300
Exp 3	7.25	01:12.5	615	14,900
Exp 4	7.25	01:12.5	615	18,300
Exp 5	7.25	01:17.5	445	14,900
Exp 6	7.25	01:17.5	445	18,300
Exp 7	7.25	01:17.5	615	14,900
Exp 8	7.25	01:17.5	615	18,300
Exp 9	11.07	01:12.5	445	14,900
Exp 10	11.07	01:12.5	445	18,300
Exp 11	11.07	01:12.5	615	14,900
Exp 12	11.07	01:12.5	615	18,300
Exp 13	11.07	01:17.5	445	14,900
Exp 14	11.07	01:17.5	445	18,300
Exp 15	11.07	01:17.5	615	14,900
Exp 16	11.07	01:17.5	615	18,300
Exp 17	5.85	01:15	530	16,600
Exp 18	13.58	01:15	530	16,600
Exp 19	9.04	01:10	530	16,600
Exp 20	9.04	01:20	530	16,600
Exp 21	9.04	01:15	360	16,600
Exp 22	9.04	01:15	700	16,600
Exp 23	9.04	01:15	530	13,200
Exp 24	9.04	01:15	530	20,000
Exp 25	9.04	01:15	530	16,600
Exp 22	9.04	01:15	700	16,600
Exp 23	9.04	01:15	530	13,200
Exp 24	9.04	01:15	530	20,000
Exp 25	9.04	01:15	530	16,600

Table 1 lists the conditions selected for each experiment. Raw curcumin was weighed and solubilized in ethanol (solvent). The curcumin ethanolic solution was then rapidly mixed with Milli-Q water (anti-solvent) at room temperature in a 1 L beaker in one step addition. While pouring the ethanolic solution, the water was stirred using an Ultra-Turrax (IKA) device to create fast mixing and homogeneous supersaturation. The mixture was stirred an additional 5 min to ensure equilibrium after the curcumin crystals precipitation. The resulting dispersion was filtered under vacuum using a Büchner flask, funnel, and filter paper (90 mm diameter) to separate the particles formed from the saturated solution. The filter cake was washed with water and completely dried in open air for 24 h. Both the curcumin raw material and curcumin recrystallized powders obtained (named curcumin recrystallized from now on in this paper) have been subjected to extensive characterization as described in the following sections.

2.4. Characterization of curcumin crystals

Raman Microscopy: To check the homogeneity of the curcumin recrystallized powders, Raman spectra and spatial maps were acquired at room temperature using a confocal Raman microscope Horiba LabRAM HR Evolution. A 785 nm laser was used as the excitation source, and the Raman signal was collected with a Synapse Plus BIDD Detector (1024 x256 pixels), using a 300/nm grating. No filter was applied, and the laser power was set at 50 % of the maximum. Several milligrams of material were placed on a glass slide, the powder was gently pressed and scanned in a grid pattern using the 5X objective. The sampling parameters were set to get 5 acquisitions with an exposure time of 0.5 s, and a total of 100 points were measured for each sample.

To check the kinetic stability of the recrystallized powder in water, a total of 150 mg of recrystallized curcumin was dispersed in 200 mL of Milli-Q water in a 250 mL graduated jacketed reactor. The dispersion was maintained in agitation using magnetic stirring at 400 rpm for 63 h. A Huber Ministat 230 (Huber, Germany) was used to control and maintain the temperature constant at 25 °C. The dispersion was

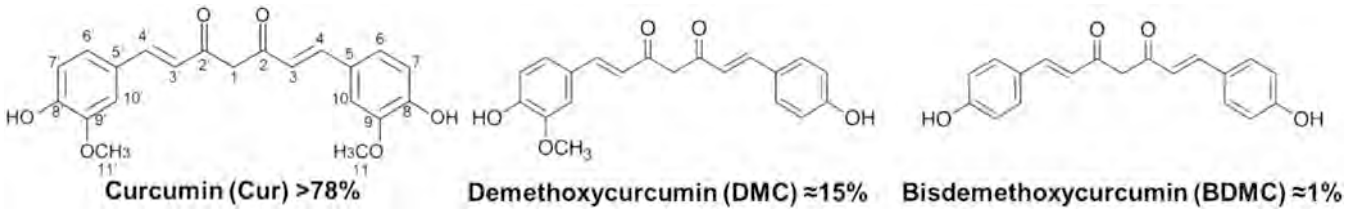

Fig. 1. Curcuminoids molecular structure and relative amount of curcuminoids in the mixture. Atom numbering of the keto-enolic form of curcumin is reported.

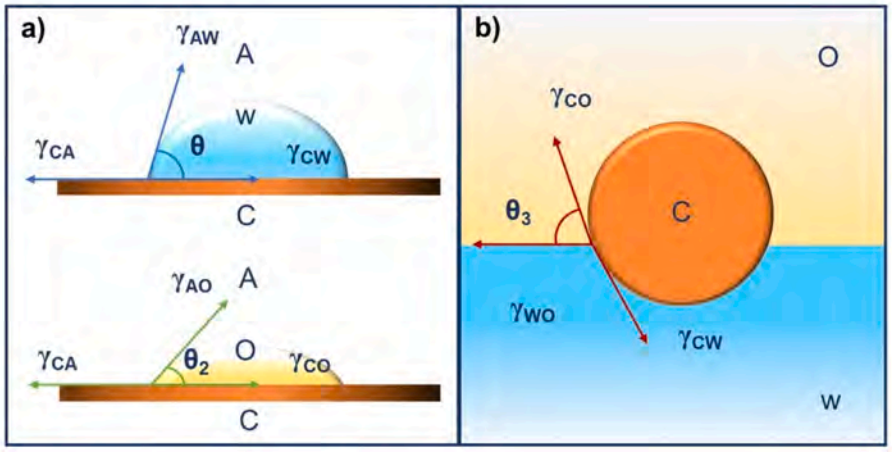

Fig. 2. Schematic of surface tensions and contact angles for: air (A), water (W) and curcumin (C) and air, oil (O) and curcumin (a); and oil, water and curcumin (b).

Table 2
Experimental condition tested for the preparation of W/O emulsions.

Experiment #	Oil (g)	Water (g)	pH	Curcumin (mg)	Mixing (rpm)
Emu W/O 1	4.73 (94.6 wt%)	0.25 (5 wt%)	7	20 (0.4 wt%)	Handshaking
Emu W/O 2	4.73 (94.6 wt%)	0.25 (5 wt%)	7	20 (0.4 wt%)	Ultra-Turrax 5000
Emu W/O 3	4.73 (94.6 wt%)	0.25 (5 wt%)	7	20 (0.4 wt%)	Ultra-Turrax 10,000
Emu W/O 4	4.73 (94.6 wt%)	0.25 (5 wt%)	3	20 (0.4 wt%)	Handshaking
Emu W/O 5	4.73 (94.6 wt%)	0.25 (5 wt%)	3	20 (0.4 wt%)	Ultra-Turrax 5000
Emu W/O 6	4.73 (94.6 wt%)	0.25 (5 wt%)	3	20 (0.4 wt%)	Ultra-Turrax 10,000
Emu W/O 7	4.48 (89.6 wt%)	0.5 (10 wt%)	7	20 (0.4 wt%)	Handshaking
Emu W/O 8	4.48 (89.6 wt%)	0.5 (10 wt%)	7	20 (0.4 wt%)	Ultra-Turrax 5000
Emu W/O 9	4.48 (89.6 wt%)	0.5 (10 wt%)	7	20 (0.4 wt%)	Ultra-Turrax 10,000
Emu W/O 10	4.48 (89.6 wt%)	0.5 (10 wt%)	3	20 (0.4 wt%)	Handshaking
Emu W/O 11	4.48 (89.6 wt%)	0.5 (10 wt%)	3	20 (0.4 wt%)	Ultra-Turrax 5000
Emu W/O 12	4.48 (89.6 wt%)	0.5 (10 wt%)	3	20 (0.4 wt%)	Ultra-Turrax 10,000
Emu W/O 13	4.23 (84.6 wt%)	0.75 (15 wt%)	7	20 (0.4 wt%)	Ultra-Turrax 10,000
Emu W/O 14	4.23 (84.6 wt%)	0.75 (15 wt%)	3	20 (0.4 wt%)	Ultra-Turrax 10,000
Emu W/O 15	3.98 (79.6 wt%)	1 (20 wt%)	7	20 (0.4 wt%)	Ultra-Turrax 10,000
Emu W/O 16	3.98 (79.6 wt%)	1 (20 wt%)	3	20 (0.4 wt%)	Ultra-Turrax 10,000

Table 3
Experimental condition tested for the preparation of O/W emulsions.

Experiment #	Oil (g)	Water (g)	Curcumin (mg)	Mixing (rpm) Dispersion Emulsification
Emu O/W 2	0.63 (5.2 wt%)	11.53 (94.7 wt%)	12.5 (0.1 wt%)	Ultra-turrax 10,000 (3 min) Ultra-turrax 10,000 (1min)
Emu O/W 2.1	0.75 (5.2 wt%)	14.25 (94.7 wt%)	15 (0.1 wt%)	Ultra-turrax 4000 (5 min) Ultrasound bath (2 min 40kHz) + Handshaking (1 min)
Emu O/W 3	0.63 (5.2 wt%)	11.53 (94.7 wt%)	6.25 (0.05 wt%)	Ultra-turrax 10,000 (3 min) Ultra-Turrax 10,000 (1min)
Emu O/W 3.1	0.75 (5.2 wt%)	14.25 (94.7 wt%)	7.5 (0.05 wt%)	Ultra-Turrax 4000 (5 min) Ultrasound bath (2 min 40kHz) + Handshaking (1 min)
Emu O/W 4	0.75 (5 wt%)	14.25 (95 wt%)	45 (0.3 wt%)	Ultra-Turrax 4000 (5 min) Ultrasound bath (2 min 40kHz) + Handshaking (1 min)
Emu O/W 5	1.5 (10.5 wt%)	12.75 (89.3 wt%)	15 (0.1 wt%)	Ultra-Turrax 4000 (5 min) Ultrasound bath (2 min 40kHz) + Handshaking (1 min)
Emu O/W 5.1	1.5 (10.5 wt%)	12.75 (89.4 wt%)	15 (0.1 wt%)	Ultra-Turrax 4000 (5 min) Ultrasound bath (2 min 40kHz) + Ultraturrax 10,000 (1 min)
Emu O/W 5.2	1.5 (10.5 wt%)	12.75 (89.4 wt%)(pH 3)	15 (0.1 wt%)	Ultra-Turrax 4000 (5 min) Ultrasound bath (2 min 40kHz) + Handshaking (1 min)

monitored in situ using a fiber-optic SuperHead Raman probe, with a 785 nm laser as the excitation source, connected to the Horiba LabRam mentioned earlier. To prevent interference from external light, the slurry, and the probe were covered in aluminium foil. One spectrum was recorded every hour, to monitor possible changes in solid form. The acquisition parameters were set to collect 20 acquisitions with 10 s exposure time. The effects of cosmic rays in the spectra were manually removed.

Powder X-ray Diffraction (PXRD): PXRD analysis was performed using a Panalytical X'Pert PRO diffractometer set up in Bragg–Brentano mode with Cu Kα radiation (λ = 1.5406 Å). The samples were gently ground in a mortar with an agate pestle and loaded onto a silicon zero-background sample holder, and diffraction patterns were recorded over a 2θ range of 4° to 40° with a step size of 0.026° and an acquisition time of 180 s per step. The obtained diffraction patterns were compared with the simulated X-ray patterns obtained from the polymorphs crystal

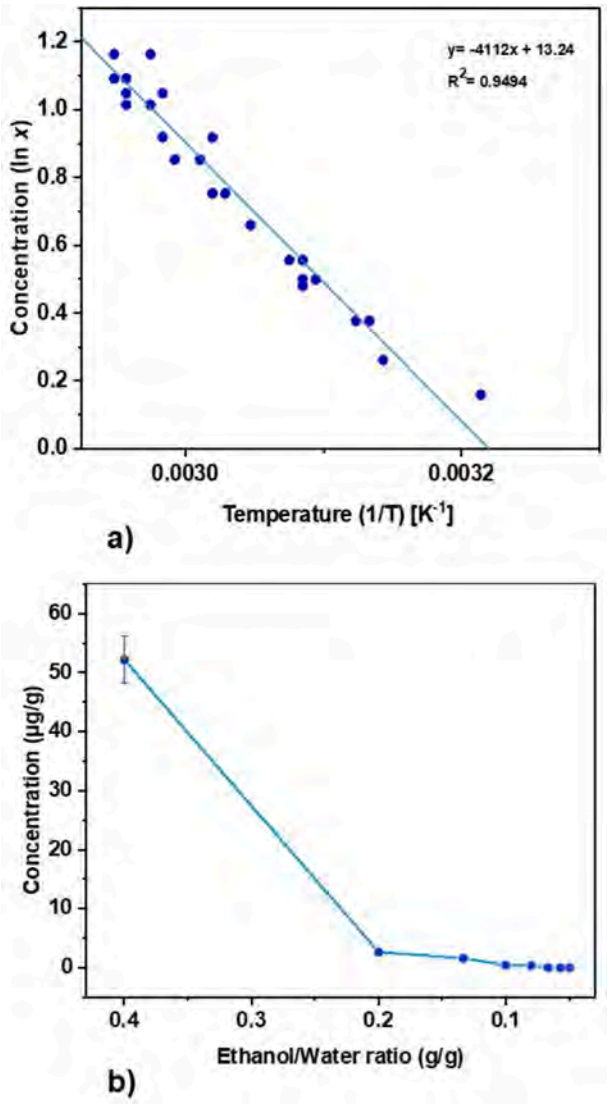

Fig. 3. (a) Van't Hoff type plot of curcumin solubility in ethanol in the range 35–65 °C. In the y axis, concentration of curcumin as natural logarithm of the molar fraction (x), in the x axis the reciprocal of temperature in Kelvin. (b) Solubility curve of curcumin as a function of increasing water content. The amount of water increases from left to right.

structures deposited in the Cambridge Structural Database (CSD), refcodes BINMEQ13, BINMEQ12 and BINMEQ07 for form I, II and III, respectively.

Solid-State Nuclear Magnetic Resonance (SSNMR): ^{13}C CPMAS (*Cross-Polarization Magic Angle Spinning*) SSNMR spectra were acquired with a Bruker Avance II 400 Ultra Shield instrument, operating at 400.23 MHz for ^{1}H and 100.63 MHz for ^{13}C. The powder samples were packed into cylindrical zirconia rotors with a 4 mm o.d. and 80 µL volume without further preparations or treatments. ^{13}C spectra were acquired at room temperature at a spinning speed of 12 kHz using a ramp cross polarization (CP) pulse sequence with a 90° ^{1}H pulse of 3.8 µs, a contact time of 3 ms, optimized recycle delays of 3.94 and 3.6 s for raw curcumin and the recrystallized sample respectively, and a number of scans equal to 1000. The two-pulse phase modulation (TPPM) scheme was used for heteronuclear decoupling, with a radio frequency field of 65.8 kHz. The ^{13}C chemical shift scale was calibrated through the methyl signal of the external standard adamantane (at 38.48 ppm with respect to tetramethyl silane, TMS).

Differential Scanning Calorimetry (DSC): DSC analysis was performed using a Mettler Toledo 8000 DSC-1 calorimeter. Approximately 2.5 mg of each sample was placed in a 40 µL aluminium pan, covered with a perforated lid. The samples were heated from 25 °C to

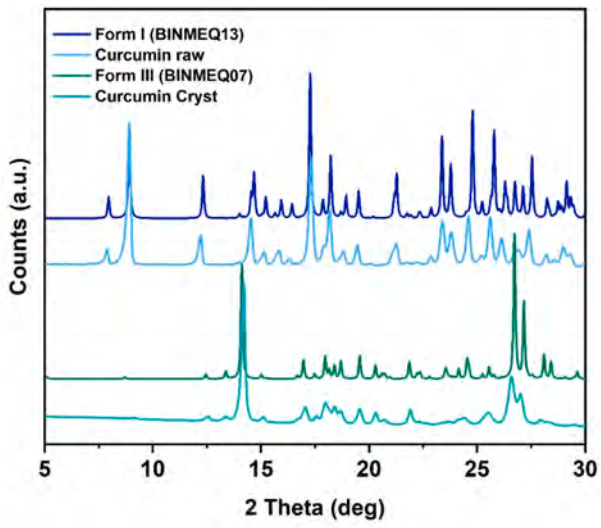

Fig. 4. PXRD pattern of raw curcumin (top) and recrystallized curcumin (bottom). The experimental patterns are compared with the simulated pattern obtained from CSD database.

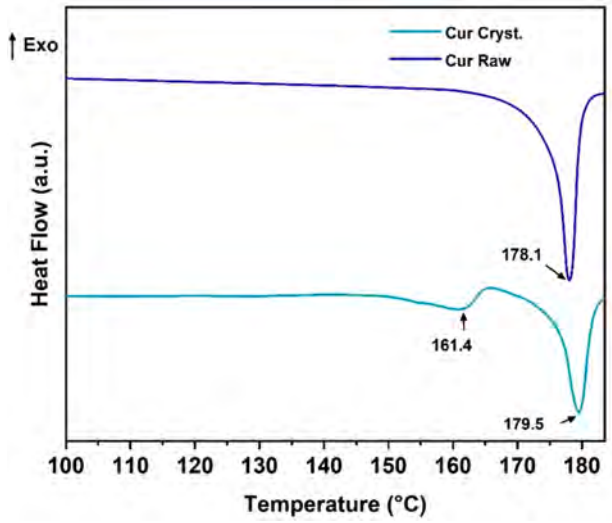

Fig. 5. DSC thermogram of raw curcumin (top) and recrystallized curcumin (bottom).

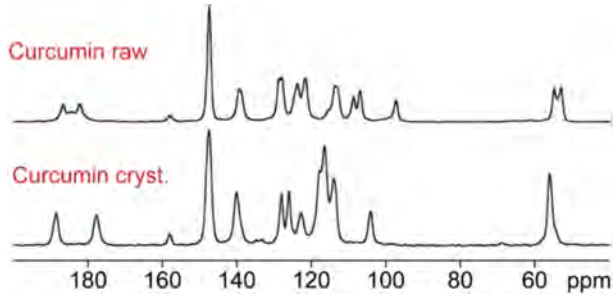

Fig. 6. ^{13}C (100.63 MHz) CPMAS spectra of the raw (top) and recrystallized curcumin (bottom) acquired at a spinning speed of 12 kHz.

Table 4
^{13}C chemical shifts of signals C2 and C2′ for the three known curcumin polymorphs (Dai et al., 2020).

	^{13}C CPMAS SSNMR – Chemical shift (δ, ppm)		
	Form I	Form II	Form III
C2	187.4	189.6 186.2	190.2
C2′	182.7	179.2 177.8	177.8

185 °C at a heating rate of 10 °C/min under a nitrogen atmosphere and then cooled to 20 °C, at a cooling rate of 10 °C/min.

Scanning Electron Microscopy (SEM): The crystal morphology and particle size distribution of the recrystallized curcumin samples were assessed through image analysis performed with a Zeiss Merlin Field Emission Gun Scanning Electron Microscope. Dry particles were finely dispersed using a spatula then fixed onto SEM specimen stubs. A platinum coating was deposited to improve sample conductivity for better image quality. The coating procedure lasted for 30 s at 30 mA. The acquired SEM images were subjected to analysis using ImageJ (version 1.52 g) software. Images were manually segmented. Binarization was applied to convert the images into binary format, and the dimensions (length and width) of the particles were obtained through the software tools. Due to the needle-like/rod-shaped morphology of the particles, an ellipse was fitted to each particle (ImageJ default function "Fit ellipse"), and the minimum and maximum lengths were considered to calculate the aspect ratio and Feret's diameter (called "equivalent diameter" from now on). An example of the workflow used for image analysis is shown in Supporting Info Fig. S1. To ensure statistical reliability, a minimum of 300 particles were selected for each sample as shown in (Fig. 1).

2.5. Computational analysis of curcumin crystal structures

The crystallographic information files (.cif) for the two curcumin polymorphs structures (form I and form III) used in the analysis were obtained from the Cambridge Structural Database (CSD), refcode BINMEQ13 for form I, refcode BINMEQ07 for form III. The .cif files were analyzed with the CCDC Mercury software v.2023.1.0 (Macrae et al., 2008). The optimization of the crystal structures was performed using Materials Studio 2021 (v 21.1.1.3268). Geometry optimization was carried out with the Forcite algorithm with Dreiding force field (Liu et al., 2019). The crystal habit of the curcumin polymorphs was predicted by the growth morphology method, which gave several possible crystal faces. The crystals were sliced parallel to the morphologically important surfaces (h k l) with a depth of 2 × dhkl. A crystal segment was created as a periodic superstructure of 3 × 3 unit cells. The interactions between the molecules in the unit cell were calculated with the Crystal Graph tool of the morphology module in Materials Studio, which ranks the intermolecular interactions. Thus, the fastest growth rate of the crystal surface would be along the direction that contains the strongest interactions. The crystal surfaces that have a fast growth rate will tend to disappear; whereas, and the crystal surfaces with a slow growth rate will prevail in the final, simulated morphology. Facet-specific surface analysis of the crystal facets of the two polymorphs of curcumin was performed with the CSD-particle tool in Mercury.

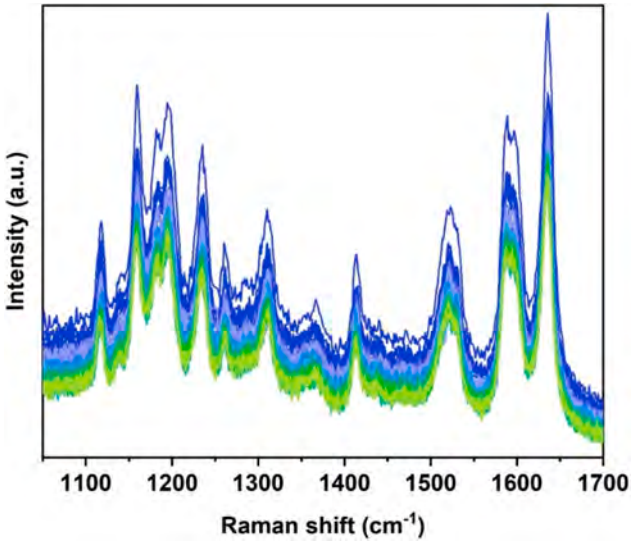

Fig. 8. In situ Raman spectra of recrystallized curcumin slurry in water over time. The slurry was monitored for 63 hr, a total of 64 spectra were recorded.

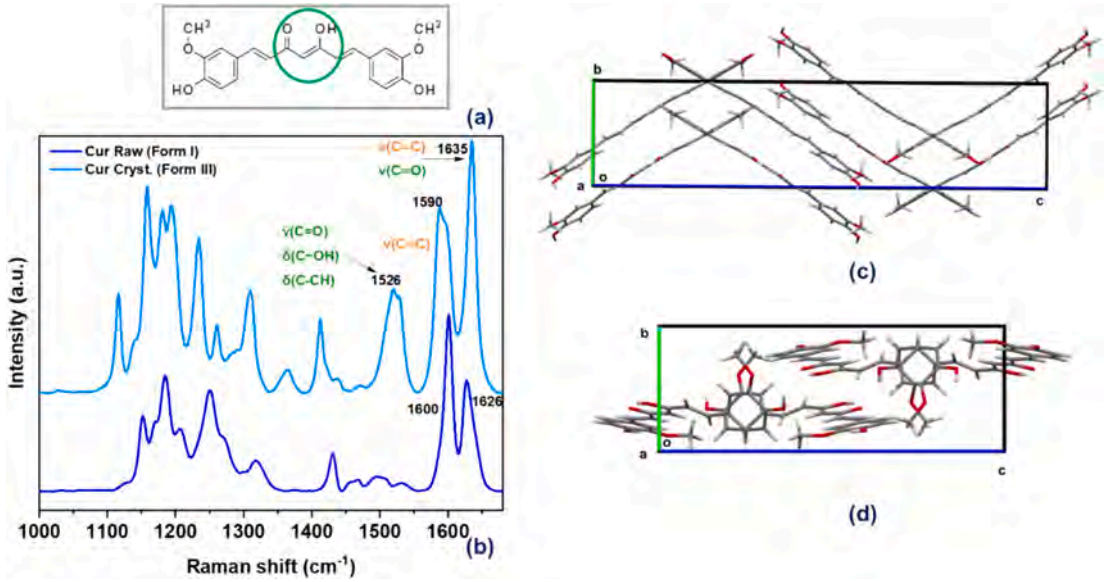

Fig. 7. (a) Curcumin molecular structure. In green the region corresponding to keto-enol tautomerism is highlighted. (b) Raman spectra of raw curcumin (on the bottom) and recrystalized curcumin (on the top), corresponding to polymorphic form I and form III, respectively. (c) Crystal packing of orthorhombic curcumin form III (BINMEQ07) and (d) monoclinic curcumin form I (BINMEQ13) along a axis.

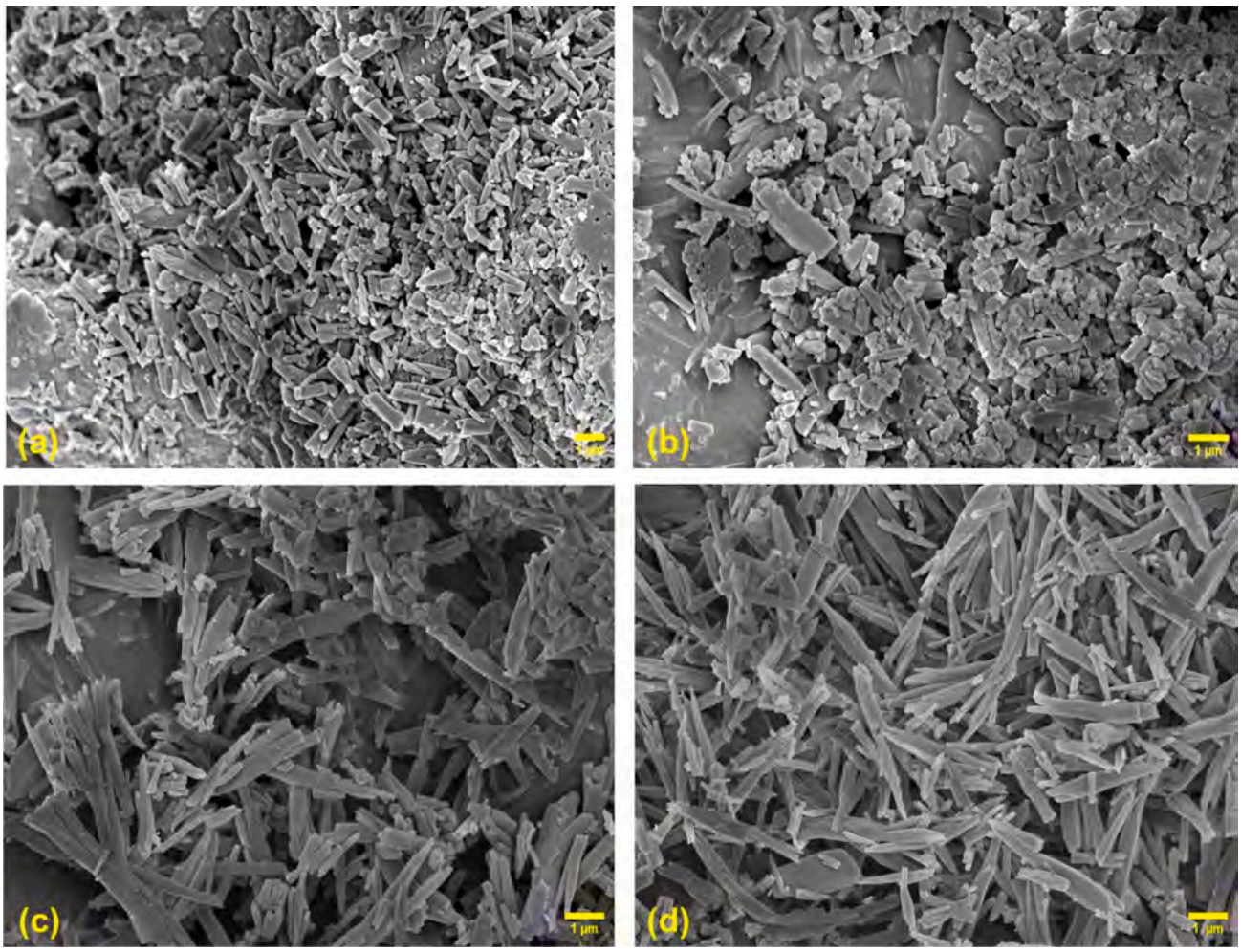

Fig. 9. Recrystallized curcumin particles observed via SEM micrographs. Crystals were from Exp 1 (conditions reported in Table 1). Images were obtained with a magnification of 20,000×, except for image (a), obtained with 15,000× magnification. Scale bars are reported for every micrograph. (a–b) show particles with a needle/rod-like morphology; (c–d) reveal the presence of dendritic, partly broken structures.

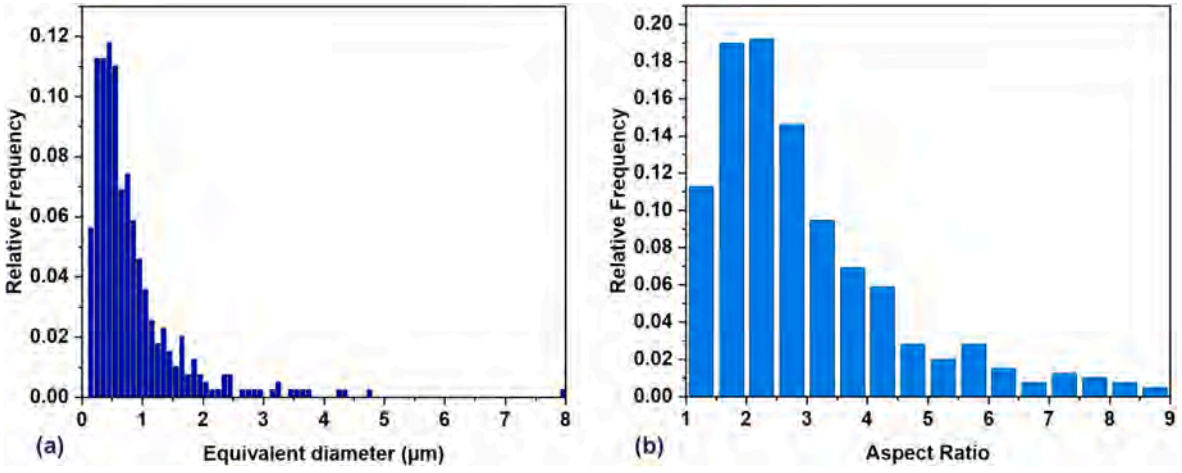

Fig. 10. Particle size and morphology distributions of a recrystallized curcumin sample. (a) Equivalent (Feret's) diameter and (b) aspect ratio of the particle population of Exp 1 (conditions reported in Table 1) were considered.

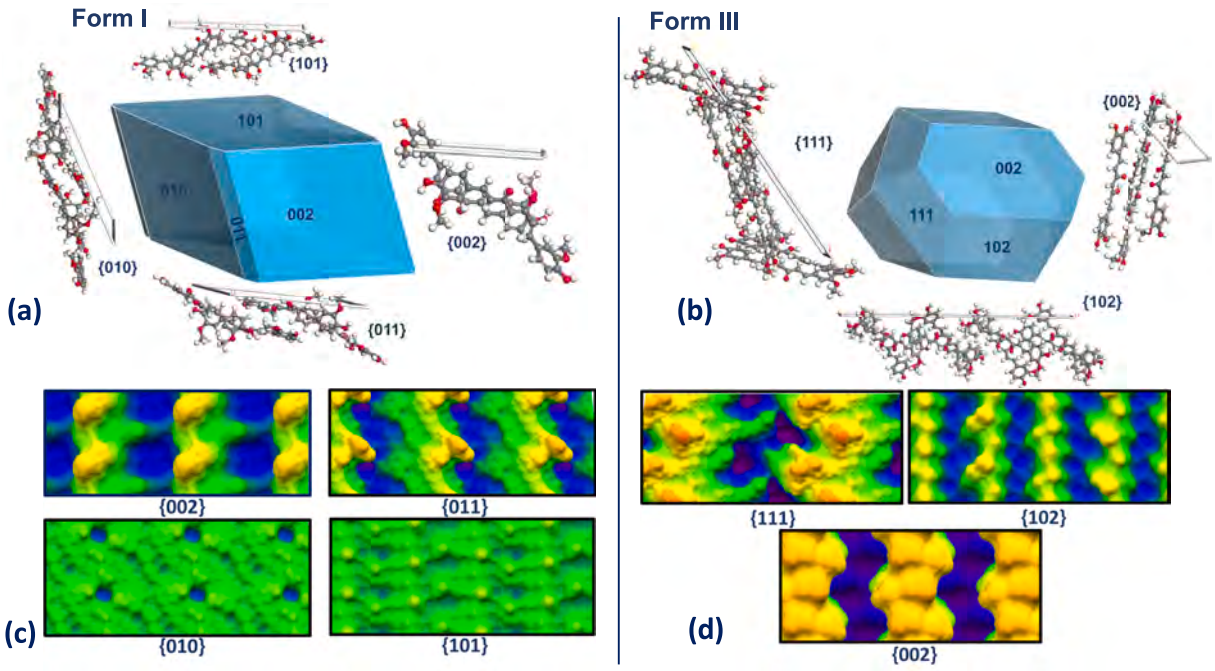

Fig. 11. Morphology prediction and facet-specific topologies calculated using the attachment energy model for curcumin form I (a) and form III (b). For the two morphologies, the topology of the most dominant facets is reported. (c) and (d) show the surface analysis of the most dominant facets, expressed as the ratio between effective and projected surface. Green regions are in line with the average plane considered by calculations, while yellow/orange and blue/purple represent surfaces respectively above and below the average plane.

Table 5
Attachment energy calculation, surface roughness and percentage areas of the most dominant facets relative both to curcumin polymorphs form I and form III.

	hkl	d_{hkl}	Eatt (Total) (kcal/mol)	Eatt (vdW) (kcal/mol)	Eatt (Electrostatic) (kcal/mol)	Eatt (H-bond) (kcal/mol)	% Total facet area	Roughness
Form I	{101}	11.11	−63.9	−61.3	0	−2.6	5.1	1.244
	{101}	10.25	−26.8	−25.5	0	−1.3	42.4	1.196
	{002}	9.92	−40.8	−39.5	0	−1.3	24.2	1.780
	{010}	7.18	−45.3	−44.3	0	−1.0	23.1	1.627
Form III	{002}	17.23	−104.3	−61.5	−27.6	−15.2	30.7	1.686
	{102}	10.14	−130.5	−67.1	−27.6	−35.9	35.2	2.980
	{111}	6.61	−178.4	−113.5	−36.7	−28.3	34.1	1.693

Table 6
The contact angle values for raw curcumin and recrystallized curcumin are reported. Water at pH 7, pH 3 (adjusted with HCl 0.1 M) and MCT oils were tested.

	Water (θ_1 pH 7)	Water (θ_1 pH 3)	Oil (θ_2)
Cur Raw (form I)	90.0° ± 5.0°	84.3° ± 10.3°	29.0° ± 0.7°
Cur (form III)	62.4° ± 6.4°	63.3° ± 1.9°	24.4° ± 2.5°

2.6. Contact angle measurements

The wettability of both the raw curcumin and the crystallized particles was evaluated by measuring the contact angle through the sessile drop technique, using a DSA25 Drop Shape Analyzer (Krüss Scientific) equipped with a microsyringe and CF03 high-speed camera with CMOS sensor. Water at different pH (pH 7 and 3) and medium-chain triglyceride (MCT) oil were tested on a disk of curcumin pressed powder. Disks of approximately 100 mg were prepared by placing gently ground

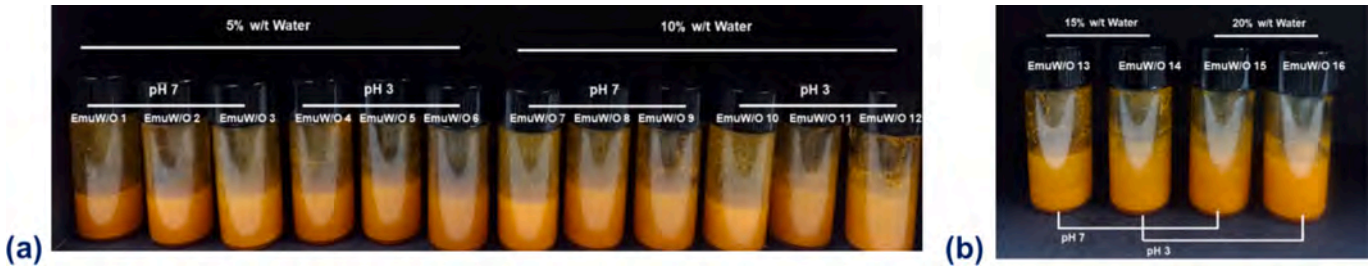

Fig. 12. W/O emulsions prepared (a) varying the mixing condition and (b) fixing the speed of agitation at 10,000 rpm. The load of curcumin particles was fixed.

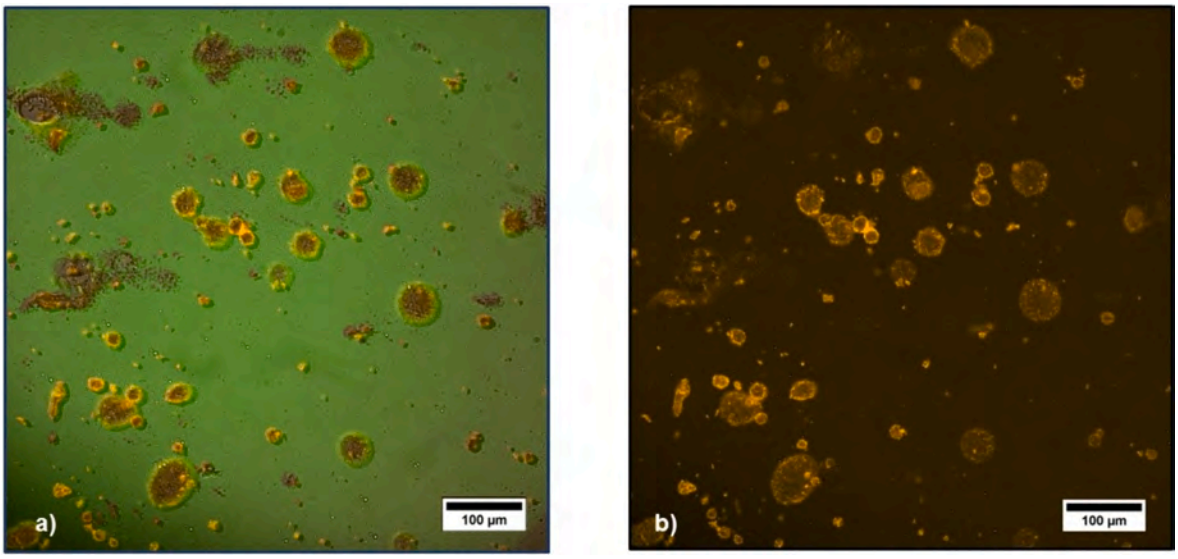

Fig. 13. Confocal images of 20 wt% W/O emulsion stabilized by curcumin particles. (a) Merged channels of brightfield, green and red emission ones and (b) red channel images were collected for the same sample. The fluorescence of curcumin (both red as solid and green in MCT oil) causes the yellow colour at interfaces, whereas the green fluorescence is caused by partial dissolution of curcumin in the oil phase.

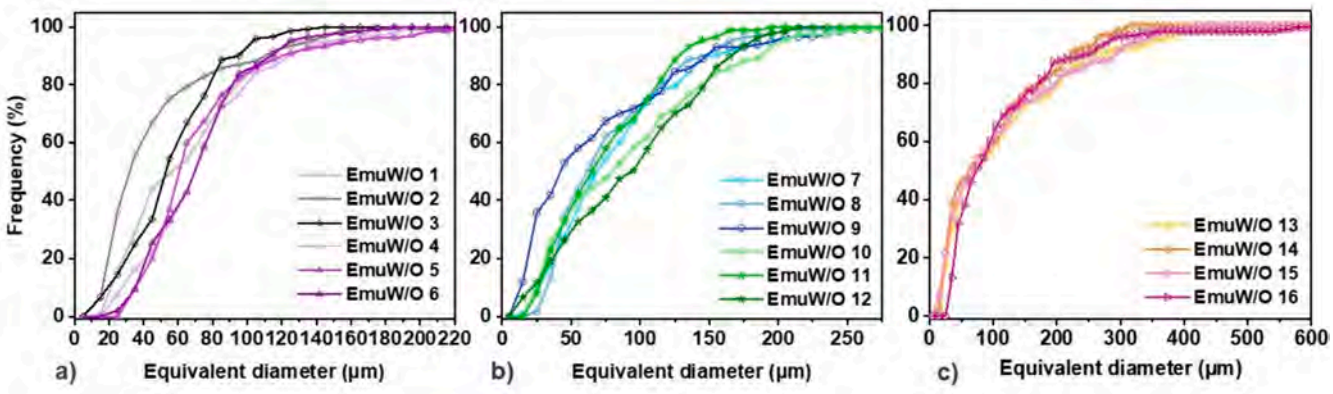

Fig. 14. Emulsions droplet size distribution represented as cumulative frequency, expressed in percentage of droplets over the total number. The samples were grouped according to water content in W/O emulsions. In graph (a) emulsions prepared with 5 wt% of water can be observed, in (b) 10 wt% and (c) 15–20 wt% water contents are shown.

powder between the plates of a hydraulic bench press with a diameter of 1.2 cm and pressing the sample under a pressure of 200 bar for 30 s. Two trace paper disks were inserted between the plates to ensure the formation of a homogeneous and smooth disc surface. The measurements were conducted at room temperature. Water and oil droplets (2 µL droplet volume) were placed onto the disk surface using a needle, and the droplet behavior was recorded with a camera. The droplet contour was analysed using the Young-Laplace method with Krüss Advance 1.12.0.35401 software, and the contact angle between the disk substrate and the water (θ_1) or oil droplet (θ_2) determined. Each measurement was performed five times to ensure accuracy. The three phase contact angle curcumin, oil and water (θ_3) was calculated from these two values using the following equations (referring to the schematic of Fig. 2):

$$\gamma_{CA} - \gamma_{CW} - \gamma_{AW}\cos\theta_1 = 0$$

$$\gamma_{CA} - \gamma_{CO} - \gamma_{AO}\cos\theta_2 = 0$$

$$\gamma_{CW} - \gamma_{CO} - \gamma_{WO}\cos\theta_3 = 0$$

where the σ values are the surface tensions among the different phases: air (A), curcumin (C) and water (W). Most of these values were taken from literature (Bhatluri et al., 2015; Fisher et al., 1985; Supran et al., 1971) and are respectively: $\gamma_{AO} = 30.14 mN/m$, $\gamma_{AW} = 72.8 mN/m$ and $\gamma_{OW} = 24.77 mN/m$. Rearranging the three previous equations we can obtain the desired value θ_3:

$$\cos\theta_3 = \frac{\gamma_{AO}\cos\theta_2 - \gamma_{AW}\cos\theta_1}{\gamma_{WO}}$$

2.7. Emulsions preparation and characterization

Preparation of W/O emulsions: Water in oil (W/O) emulsions were prepared using the conditions shown in Table 3. The curcumin particle concentration was fixed, while the effect of different amounts of water, the pH, and the speed of stirring was tested. Curcumin recrystallized particles were first dispersed in the continuous phase, MCT oil, using the Ultra-Turrax mixer, operating at 10,000 rpm for 3 min. Water was then added as the dispersed phase, at pH 7 and 3. Two different pH values, 3 and 7, were tested to appreciate differences in the interface stabilization of curcumin particles. These values were chosen to keep the product safe for human consumption. pH values greater than 7 were not considered as curcumin undergoes chemical degradation in basic environments

Table 7
Mean droplet size (diameter) and standard deviation (S.D.) calculated from image analysis using ImageJ software, as reported above for particle size distribution. The wide range of dimensions is due to the formation of smaller droplets which create a nest that stabilize bigger droplets through bridging mechanism.

	Mean (μm)	S.D. (μm)
1	68.83	38.07
2	51.75	38.97
3	60.45	27.48
4	78.40	38.01
5	77.16	39.46
6	75.64	30.68
7	87.32	53.78
8	81.52	46.26
9	71.75	60.09
10	95.74	61.86
11	97.60	40.81
12	97.13	54.04
13	119.20	109.77
14	100.44	82.05
15	114.11	103.88
16	115.81	106.89

(Priyadarsini, 2009). The aqueous phase was mixed with the oil dispersion for 1 min (experimental conditions in Table 2). After preparation, the emulsions were sealed with Parafilm and stored at room temperature in a dark place. For the preparation of the emulsions, both for W/O and O/W, curcumin crystals from experiments 13, 14, 15, and 16 reported in Table 1 were used. Although the characterization of the samples revealed no significant differences among the batches, these samples were selected because they were the most similar in terms of mean value of particle size, aspect ratio and morphology.

Preparation of O/W emulsions: Recrystallized curcumin powder was dispersed in the continuous phase (Milli-Q Water), followed by the addition of the dispersed phase (MCT oil), and the system was further mixed for several minutes. The pH of the acidic water was adjusted by adding a few drops of an aqueous solution of 0.1 M HCl. Different dispersing and emulsification methods, such as Ultra-Turrax mixing, ultrasound bath and handshaking, were tested, curcumin crystals load and amount of oil were evaluated, as reported in Table 3. The emulsions were sealed with Parafilm and stored at room temperature in a dark place.

Characterization and stability assessment of curcumin emulsions: Optical microscopy was used to measure the size distribution of the dispersed phase in the emulsions prepared with curcumin crystals. A Zeiss Axiolab 5 microscope at 5X and 10X magnifications was used for this purpose; images were collected with a digital camera with 48 Mp, resolution 4000 × 3000 pixels. The images collected were analysed using ImageJ (version 1.52 g), as described above for the crystal size distribution measurements with SEM. For each sample, the Feret diameter of 100 droplets minimum were considered.

To examine the structure of both water-in-oil (W/O) and oil-in-water (O/W) emulsion droplets, a spinning disk confocal microscope (Nikon Eclipse Ti-e fluorescence optical inverted microscope) was utilized, equipped with crest large FOV lasers and a super bright wide-spectrum source (Shutter Lambda XL), a high-resolution camera (Zyla 4.2 Plus, 4098 × 3264 pixels, Andor Technology), and a motorized stage. 10 μL of the sample was carefully placed onto a glass slide, ensuring the absence of any air gaps between the sample and the coverslip. The emulsions were gently agitated before the measurement to ensure homogeneity. Brightfield, green and red emission images, recorded with a light excitation of 488 nm and 550 nm, respectively, were acquired using a 20x objective (Nikon). In order to assess the stability against coalescence of the prepared emulsions, all samples were kept at room temperature and protected from light for several months. Samples were periodically checked visually to observe phase separation, and with optical microscopy to quantify droplet size distribution.

3. . Results & discussion

3.1. Curcumin crystals preparation and characterization

Sub-micrometer curcumin crystals were successfully produced via anti-solvent crystallization. The chosen anti-solvent technique and the parameters tested aimed to maximize supersaturation conditions, promoting nucleation over growth (Meenan, 2001), and yielding small crystals with narrow size distribution. A high yield of recovery from the liquid, ranging from 80 % to 94 % w/w (ratio between starting material weight and recovered powder weight) was also favoured with this method (data in Supporting Info, Table S3). To define the crystallization parameters to test, in terms of solute concentration and solvent-antisolvent ratio, previous solubility measurements of curcumin in ethanol and in ethanol–water analytes with increasing water content were performed. Fig. 3 *a* and *b* show respectively the solubility of raw curcumin in ethanol at different temperatures (ter Horst et al., 2009) and the solubility of curcumin in ethanol–water mixtures. Further information related to this data is shown in Supporting Information Fig. S2. Upon resuspension in water of the obtained crystals, a fine, homogeneous, dispersion was formed, with a considerable improvement in ease of dispersion compared to the raw curcumin. To confirm the absence of chemical degradation or amorphization during particle formation and identify the crystal form, various analytical techniques, including Raman spectroscopy, powder X-ray diffraction (PXRD), Solid-State Nuclear Magnetic Resonance (SSNMR) and Differential Scanning Calorimetry (DSC) were used. The analyses were conducted on the recrystallized samples and the raw untreated material for comparison. The particle morphology and size distribution were evaluated through SEM imaging.

The polymorphic form of the crystals obtained via anti-solvent precipitation experiments was always the metastable form III of curcumin (Thorat & Dalvi, 2014). This metastable form formation is favoured by the high supersaturation achieved at high water to ethanol solution ratios (Coquerel, 2014; Roelands et al., 2006), and with the rapid mixing provided by the UltraTurrax. The crystallized material exhibited a characteristic red–orange colour compared to the yellow-orange of the raw curcumin (Supporting Info, Fig. S3), which was found to be stable form I of curcumin.

The formation of polymorph form III was confirmed by PXRD analysis and comparing the collected powder patterns to the calculated ones from crystallographic data from the literature (Fig. 4). The PXRD diffractograms show high crystallinity (e.g., sharp peaks) of the curcumin particles obtained from anti-solvent precipitation, and homogeneity in terms of polymorphism. DSC thermograms of raw and recrystallized curcumin (form I and form III) are presented in Fig. 5. Form I exhibits an endothermic peak at 178 °C, corresponding to melting of the sample. In the thermogram of form III, the first peak at 161 °C corresponds to an endothermic solid-state transformation to form I, as confirmed by other studies (Pandey & Dalvi, 2019; Thorat & Dalvi, 2015). The second endothermic peak at 179.5 °C corresponds to the melting of form I (Sanphui et al., 2011; Thorat & Dalvi, 2015). The slightly different onset of melting between the two samples can be attributed to the different particle sizes (Lee et al., 2001).

Due to the high similarity between the diffraction patterns of curcumin form II and III (Sanphui et al., 2011), SSNMR analysis was also performed to further confirm the polymorphic form of the anti-solvent curcumin crystals. This solid-state characterization technique allows discerning different crystalline forms with great accuracy due to its high sensitivity to the chemical surroundings of the nuclei constituting the system (Chierotti et al., 2010).

The most important structural difference between forms II and III is the number of independent molecules: one for the latter ($Z = 8$, $Z' = 1$), as in form I, and two for form II ($Z = 8$, $Z' = 2$), making them easily distinguishable by SSNMR (Dai et al., 2020). In fact, Z' = 2 results in a splitting of all signals in the spectrum, except for some casual

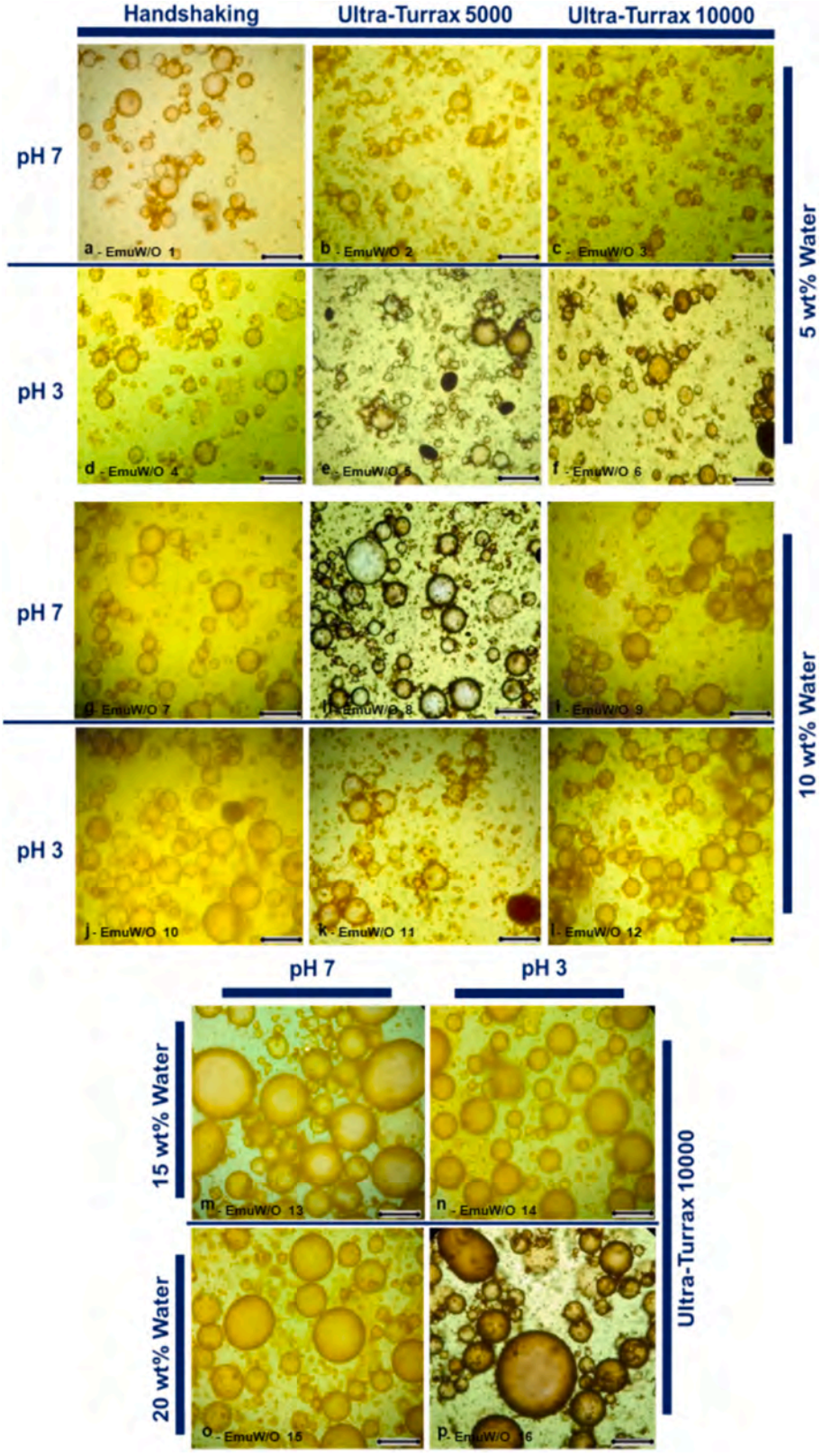

Fig. 15. Images of W/O emulsion obtained through optical microscope. The scalebar is set to 250 μm for all the samples.

overlapping. Fig. 6 shows the ^{13}C CPMAS SSNMR spectra of raw and recrystallized curcumin.

Only two signals can be observed for C2 and C2′ (Fig. 1). More than any others these signals allow a distinction between the different polymorphic forms: for raw curcumin they are found at 187.1 and 182.6 ppm, while for recrystallized curcumin at 188.9 and 177.9 ppm. These results are in good agreement with what has been reported in the literature for form I and III, respectively (Table 4) (Dai et al., 2020), indicating that the raw curcumin mainly consists of curcumin form I, while the recrystallized one of form III. The presence of single signals for

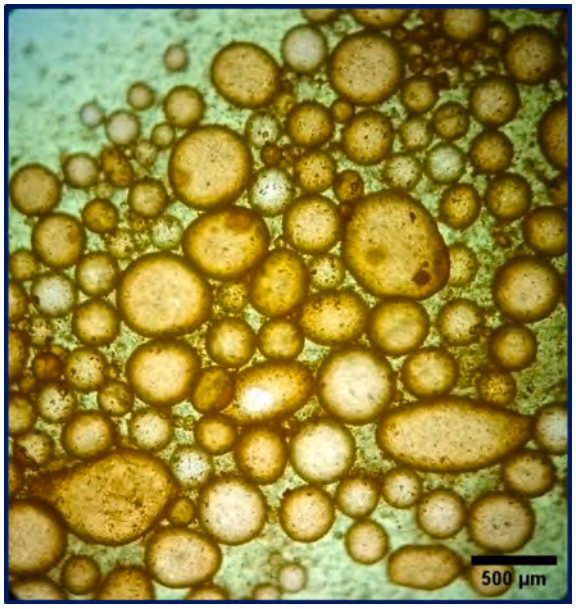

Fig. 16. Emulsion Emu W/O 16 after 4 months of storage. Optical microscopy reveals an enlargement of the droplets and particle dispersed in the continuous phase.

Fig. 17. Sample Emu W/O 16 left in air on a glass slide for 30 min. The resulting deflated structure demonstrates that the particles are strongly adsorbed at the interface.

the two expected C atoms in this region definitively rules out the formation of form II, for which a number of signals of four, two for C2 and two for C2′, is expected. However, spurious signals are observed in both ^{13}C CPMAS spectra: at 184.9 ppm and 158.8 ppm for raw curcumin and at 158.4 ppm for the recrystallized one. These impurities are likely due to the presence of curcumin derivatives, such as demethoxycurcumin and bisdemethoxycucrcumin (Siudem et al., 2023). As mentioned earlier, given the absence of involvement of curcumin methoxy groups in H-bonds or significant intramolecular interaction that can be responsible for molecular torsion, the presence of these derivatives should not affect greatly the properties of the compound.

Raman microscopy was used to obtain 2D maps of all the curcumin crystals obtained via anti-solvent precipitation to verify the homogeneity of the samples. Fig. 7 shows the Raman spectra of form I and form III. The latter exhibits a unique peak at 1532 cm^{-1}, corresponding to intermolecular interactions in the central keto-enol region. Form I shows enhanced ν(C═C) stretching vibrations. These two peaks were used to unequivocally identify the two forms (Prasad et al., 2020) in each collected map. All samples were found to be homogenous in terms of polymorphism, with only form III detected in all spectra collected for each map (example of measurement shown in Supporting Info, Fig. S4).

As the recrystallized form III is thermodynamically unstable at ambient conditions we checked for its kinetic stability (e.g., slow kinetic of polymorphic transformation) in both air and water. In fact, a kinetically stable solid can still be used for Pickering formulations. Form III samples did not show polymorphic changes when stored at room conditions in a dark place for over 10 months. In situ Raman was used to check kinetic stability of form III in water slurry; Fig. 8 shows that no significant differences in Raman spectra were observed over the 63 hr of the experiment, indicating the absence of phase transformation or degradation of curcumin crystals. Slurries of curcumin in water were further checkeded after 3 months and showed the persistence of form III. Therefore, it can be concluded that form III has reasonable kinetic stability and may be used in Pickering formulations with relatively long shelf-life.

SEM images of recrystallized curcumin particles obtained from one batch (Exp 1, Table 1) are reported in Fig. 9. Crystals show fairly narrow size and shape distributions, predominantly exhibiting a needle/rod-like shape (Fig. 9*a–b*). Additionally, aggregates of crystals can be observed, potentially formed during filtration. Furthermore, dendritic structures (Fig. 9*c–d*) can be observed, likely formed due to secondary nucleation, which is influenced by the mixing conditions and the level of supersaturation used during the experiments. The high-speed rotor–stator mixing employed in this study generates shear forces and turbulent flow, facilitating mixing and mass transfer but also leading to crystal breakage and/or aggregation (Fig. 9*c–d*). Fragile crystals that grew as dendrites or needles were more prone to breakage into smaller particles.

Quantification of morphology (aspect ratio) and size distributions of crystallized curcumin particles were determined by examining SEM images at various magnifications for all 25 samples. The results for a representative experiment (Exp 1, Table 1) are graphically shown in Fig. 10; whereas the average size and aspect ratio values with their standard deviation are reported in Supporting Information Table S3. The crystallized samples exhibited a narrow distribution of equivalent diameters, ranging from 0.5 to 1.2 μm, with a mean aspect ratio ranging from 1.6 to 3.5. Supporting Information Fig. S5 shows the results of the statistical analysis performed on the size and shape average values; this analysis demonstrates that there is no significant relationship between the operating parameters (e.g., stirring rate, volume ratio) explored and the resulting particle size and morphology, within the chosen design space. This might be related to the fact that similar high levels of curcumin supersaturations were used in all experiments, despite changes in solvent to antisolvent ratios and curcumin initial concentrations. At such high levels of supersaturations, it is possible that the effect of other operating conditions on crystal size and shape distributions might be negligible.

A noticeable reduction in particle size was observed when comparing the shape and size of the curcumin crystallized via anti-solvent with the raw material provided by the supplier (mean equivalent diameter of 3.8 μm and mean aspect ratio of 1.4). Additionally, the higher average aspect ratio in the recrystallized samples indicated a more acicular shape of anti-solvent crystallized curcumin compared to the raw material.

The interfacial behaviour of curcumin particles (raw and from anti-solvent crystallization) was determined through contact angle measurements (θ_1 and θ_2), which are reported in Table 6. Curcumin raw powder (form I) showed a hydrophobic nature with a value of θ_1 of around 90°, and more affinity with the oil phase (θ_2 around 29°). The recrystallized form III has similar affinity to oil (θ_2 is about 24°) but shows a more hydrophilic nature with an average value of θ_1 of 62.4°. Non-significant differences in values of θ_1 were observed with water at different values of pH. The values of measured contact angle explain the

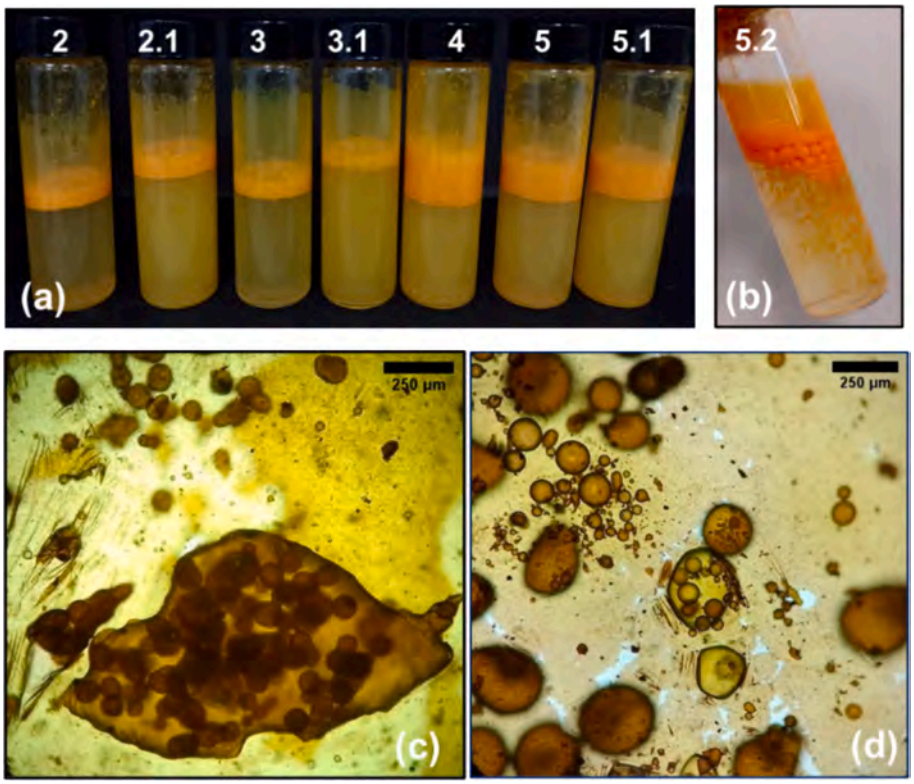

Fig. 18. In O/W emulsions from 2 to 5.1 reported (a) water at pH 7 was used while (b) 5.2 sample was prepared with water at pH 3. Images obtained through optical microscope of sample 2 (c) and sample 5.1 (d) are reported.

better dispersibility of the recrystallized form III in water, compared with the raw form I material. The minimum calculated θ_3 value (considering the measurement standard deviation) for form I at pH=7 is around 36°, which indicates suitability for water in oil emulsion stabilization. The θ_3 value for the recrystallized curcumin ranges from 81 to 124°, which indicates the potential of curcumin particles for stabilization of both O/W and W/O emulsions. It is worth noticing the considerably higher standard deviation of the measurements conducted on form III with water compared to form I. This might be related to the smaller size of the recrystallized particles, which significantly affected the quality of the compressed disk (e.g., higher surface roughness, difficulties in powder handling). Despite the larger standard deviation, the higher hydrophilicity of form III is evident. This is likely related to the different molecular terminations characterizing the facets of the two curcumin polymorphs. In fact, different polymorphs of the same compound can expose different functional groups of their constituting molecules on their facets, affecting facet-specific surface properties. Additionally, it has been reported that polymorphs usually differ in surface roughness (Montis et al., 2020), which can also affect wettability. To verify this hypothesis a computational study of the two crystal structures was performed using Mercury and Materials Studio. Fig. 11 shows the predicted morphology of curcumin form I and form III (Fig. 11 *a* and *b*) and a graphical representation of the simulated topology for the largest facets identified (Fig. 11 *c* and *d*). As visible from Table 5, both the polymorphs show a high contribution of van der Waals interactions (i.e., π-π stacking) for all the crystal facets. The contribution of hydrogen bonds and electrostatic interactions to the total lattice energy is minimal for form I. Indeed, as shown in Fig. 11 *a*, neither of the facets' termination shows any hydrogen bond acceptor or donor groups (e.g. methoxy and hydroxy groups). On the other hand, curcumin form III shows a slightly higher contribution of both hydrogen bonds and electrostatic interactions to the total lattice energy; this is demonstrated by the presence of hydrogen acceptor and donor groups on most of form III facets (Fig. 11 *b*). Comparing the surface topologies of both polymorphs (Fig. 11 *c* and *d*), form III presents a higher surface roughness compared to form I (more details are given in Supporting Info Fig. S6 and Fig. S7). The computational analysis is, therefore, in agreement with the experimental data that indicates a more hydrophilic nature of curcumin form III compared to form I.

3.2. Emulsions preparation and characterization

Water-in-oil (W/O) emulsions were prepared using the conditions reported in Table 3. Fig. 12 shows the visual appearance of the prepared emulsions, which did not show evident phase separation for solid particles and the two liquid phases. It is worth noticing that water droplets sedimentation was observed within a few minutes of preparation of the W/O emulsions, due to the large average size of the dispersed phase. Confocal fluorescence microscopy of the samples was performed to check the type of the formed emulsion and to assess the interfacial activity of curcumin particles. Fig. 13 clearly shows that a Pickering stabilized W/O emulsion is formed; water droplets are surrounded by curcumin particles adsorbed at the water/oil interface. The yellow color is due to the colocalization of curcumin emitting both in the green channel, when dissolved in MCT oil, and in the red channel as solid phase (Araiza-Calahorra & Sarkar, 2019; Mondal et al., 2016). It is worth noticing that neither MCT oil nor water were stained with other dyes, hence the natural green fluorescence is due to dissolved curcumin. The arrangement of curcumin particles around the water droplets indicates the typical droplet bridging of Pickering emulsions (French et al., 2015), which provides improved stability to the droplets and reduces coalescence over time.

The size distribution of water droplets in each emulsion sample was measured via optical light microscopy. All droplet size distributions are reported in Fig. 14; whereas the average values with corresponding standard deviations are reported in Table 7. Water droplets were found to be between 70 to ~100 µm in equivalent diameter, which is consistent with the mean size of the curcumin particles used. It can be observed

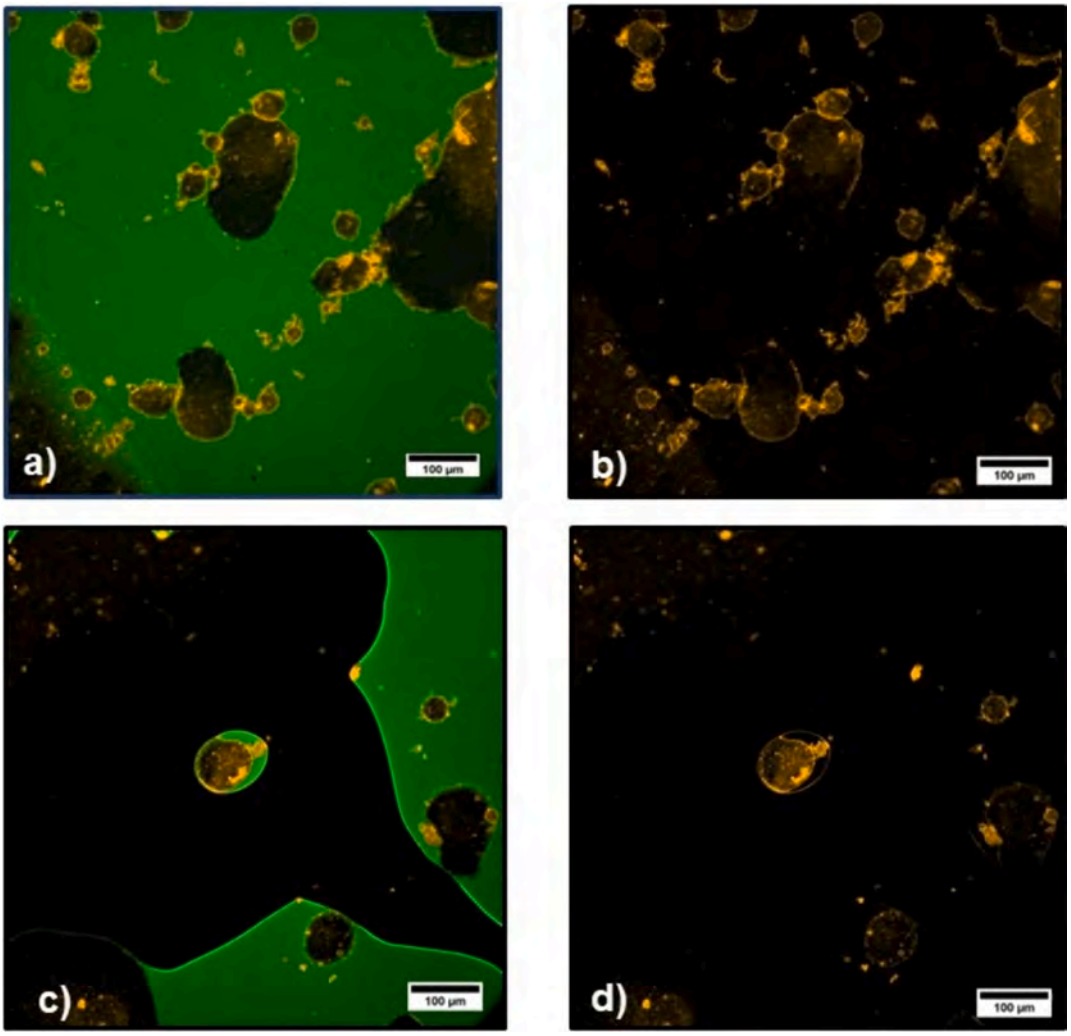

Fig. 19. Confocal images of sample emu o/w 5. The auto-fluorescence of curcumin causes the yellow brightness. Green fluorescence is caused by partial dissolution of curcumin in the oil phase. Images (b) and (d) show curcumin only autofluorescence. Images a) and c) were obtained in bright-field option.

that higher contents of water in the emulsions determined higher average droplet sizes and improved interfacial coverage by particles (as shown more clearly in Fig. 15 *m–n–o–p*). In general, all droplet size distributions are quite broad, as shown by the relatively large standard deviations ranging from 30 to over 100 μm. Increasingly broader droplet size distributions can be observed as the amount of dispersed phase in the emulsions increases, as clearly shown in Fig. 14 *a* to *c*. Nevertheless, the presence of these smaller droplets is beneficial, as they form a particle/droplet network that provides bulk stabilization to the emulsions via a bridging mechanism (as shown more in details in Supporting Info, Fig. S8).

The type of stirring had a weak effect on the average size and standard deviation of the droplets distribution; slightly larger and broader distributions were observed with handshaking compared to high-shear mixing (e.g., Emu W/O 1 vs 2, 4 vs 5 and 10 vs 11). However, in Fig. 15 it can be observed that an increase in shear resulted in a higher occurrence of droplet bridging, in agreement with previous studies reported by French et al. (French et al., 2015). Additionally, higher shear led to more uniform surface coverage from the particles and to fewer solid particles dispersed in the continuous oil phase. These observations are shown more clearly in Fig. 15 *a* to *l*. The pH of the water phase also influenced the emulsion microstructure. By comparing Emu W/O 1 and 4, and 7 and 10 (Fig. 14 and Table 7) it is possible to observe the effect of pH on droplets size distribution. Emulsions prepared with lower pH exhibited larger droplets compared to those prepared at pH 7, which is consistent with previous findings of Luo et al. evaluating the efficiency of flavonoids as stabilizers in biphasic systems (Luo et al., 2011).

A decrease in pH led to the formation of large aggregates of curcumin particles (Fig. 13 *e–f–j–k*, opaque spots), which reduced the number of available particles for interfacial stabilization.

Despite the relatively large droplets size, the W/O emulsions prepared with curcumin particles did not show significant visual changes over several weeks of storage. A representative example of long-term stability is shown in Fig. 16, which depicts the appearance of the Emu W/O 16 emulsion four months after preparation.

A further demonstration of the interfacial adsorption of curcumin particle in W/O emulsions is shown in Fig. 17, which shows sample Emu W/O 16 left on a glass slide for 30 min. The deflated shape of the partially dried water droplets is due to the presence of Pickering particles (Okada et al., 2012), which are strongly adsorbed at the interface and prevent further water diffusion and evaporation by reducing the surface available for mass transfer.

Since θ_3 of recrystallized curcumin particles from anti-solvent precipitation was found to be in a range that indicated potential for O/W stabilization, this type of emulsion was also tested. Emulsions were prepared by dispersing recrystallized curcumin particles at different wt % contents, varying the MCT oil wt%, and testing different stirring techniques, as reported in Table 2. As shown in Fig. 18 the resulting emulsions were unstable, leading to droplet coalescence, phase separation and particle precipitation within a few hours regardless of the

different parameters tested. Visual inspection of the vials revealed large droplets sizes (Fig. 18-*a*), regardless of the method of preparation and the composition. It is evident that the produced curcumin particles were not suitable for O/W stabilization; indeed, a phase inversion was observed in the produced samples (Binks, 2002). Fig. 19 shows confocal fluorescence microscope images of the orange, superficial layer visible in the vials of Fig. 18 *a*: large oil domains (in green) containing smaller water droplets surrounded by curcumin particles (in yellow at O/W interfaces) are clearly visible. Even though contact angle measurements showed no significant differences in wettability between water at different pHs, in sample Emu W/O 5.2 (Fig. 18 *b*) where water at pH 3 was used, the preference for curcumin particles to stay in the oil phase was more evident, with all the oil and curcumin particles moving on the top layer. Moreover, no particle precipitation was observed in the water phase when acidic water was used.

4. Conclusions

Crystallization techniques that enable consistent control over particle properties such as size, shape, and polymorphism are essential to produce Pickering formulations with tailored properties for many applications in the food sector. In this study, we applied crystal engineering tools and good practise to develop a robust anti-solvent crystallization method to produce submicron-sized curcumin crystals suitable for Pickering stabilization. The process developed delivered curcumin particles with a uniform average size (0.5–1.2 μm), morphology (rod–like shape), and polymorphic form (the metastable form III). The curcumin particles recrystallized via anti-solvent exhibited improved dispersibility in water and enhanced hydrophilicity compared to the raw material as purchased (stable form I). This is due to the reduced size of the crystallized particles and the facet-specific surface chemistry of curcumin form III, as shown by computational modelling of the two polymorph structures.

Various conditions were investigated in the formulation of O/W and W/O Pickering emulsions, including the water-to-oil ratio, the type of emulsification technique, and the pH of the water phase. Consistent with the findings of previous studies conducted by Zembyla et al. (Zembyla et al., 2018, 2019), it was observed that curcumin particles provided superior stabilization of W/O emulsions compared to O/W ones. Indeed, the O/W samples produced in this work were highly unstable and even show phase inversion. As expected, larger water droplets were observed at higher ratios of water to oil in emulsion, with better particle coverage and droplet bridging phenomenon that provided further bulk stabilization. An increase in the stirring energy provided for emulsification, from handshaking to Ultraturrax mixing, resulted in slightly smaller droplet size. An acidic pH determined droplet enlargement and the formation of large particle aggregates that precipitated; this is probably due to the effect of solution ions on the surface charge of curcumin particles, which can increase particle–particle interactions rather than particle-interface interactions. Despite the formation of relatively coarse emulsions (average droplet diameter up to over 100 μm), the particles remained absorbed at the W/O interface, and no phase separation was observed even after several months of storage. These findings provide a deeper understanding on how crystalline properties, particularly polymorphism, can affect the effectiveness of Pickering particles. The relationship between crystal structure and facet-specific surface chemistry and topology can be predicted with crystal engineering modelling tools; whereas specific crystallization processes can be designed to precisely deliver the desired particle properties. The work presented here is a first example of the application of a crystal engineering approach to rational design of Pickering particles and formulations.

CRediT authorship contribution statement

Giulia Del Duca: Writing – review & editing, Writing – original draft, Methodology, Investigation, Formal analysis, Data curation. **Emmanuele Parisi:** Writing – review & editing, Methodology, Investigation, Formal analysis, Data curation. **Fiora Artusio:** Writing – review & editing, Formal analysis, Data curation. **Eleonora Calì:** Writing – review & editing, Methodology, Formal analysis, Data curation. **Silvia Fraterrigo Garofalo:** Writing – review & editing, Methodology, Formal analysis. **Chiara Rosso:** Writing – review & editing, Formal analysis, Data curation. **Valentina Cauda:** Methodology, Investigation, Data curation. **Michele R. Chierotti:** Resources, Methodology. **Elena Simone:** Writing – review & editing, Supervision, Resources, Methodology, Funding acquisition, Conceptualization.

Declaration of competing interest

The authors declare that they have no known competing financial interests or personal relationships that could have appeared to influence the work reported in this paper.

Data availability

Data will be made available on Zenodo.

Acknowledgments

This project has received funding from the European Research Council (ERC) under the EuropeanUnion's Horizon 2020 research and innovation programme (grant agreement No. 949229, CryForm). M.R.C. and C.R. acknowledge support from the Project CH4.0 under the MUR program "Dipartimenti di Eccellenza 2023-2027" (CUP: D13C22003520001). The authors thank the Cambridge Crystallographic Data Centre for providing the Mercury license. The authors wish to express their appreciation to Janine Andrea Preston, Cecilia Fiore and Pierfrancesco Latorre for their expertise and assistance throughout all aspects of our study. Professor Antonio Buffo is aknowledged for useful discussion on surface tension and three phase contact angles.

Appendix A. Supplementary material

Further details on Design of Experiment (DoE) and responses analysis, particle size distribution determination, HPLC calibration curve of curcumin ethanolic solution, curcumin crystal simulated facet topology and water-in-oil emulsion details. Supplementary data to this article can be found online at https://doi.org/10.1016/j.foodres.2024.114871.

References

Aditya, N. P., Hamilton, I. E., & Norton, I. T. (2017). Amorphous nano-curcumin stabilized oil in water emulsion: Physico chemical characterization. *Food Chemistry, 224*, 191–200. https://doi.org/10.1016/j.foodchem.2016.12.082

Albert, C., Beladjine, M., Tsapis, N., Fattal, E., Agnely, F., & Huang, N. (2019). Pickering emulsions: Preparation processes, key parameters governing their properties and potential for pharmaceutical applications. *Journal of Controlled Release, 309*, 302–332. https://doi.org/10.1016/j.jconrel.2019.07.003

Araiza-Calahorra, A., & Sarkar, A. (2019). Pickering emulsion stabilized by protein nanogel particles for delivery of curcumin: Effects of pH and ionic strength on curcumin retention. *Food Structure, 21*, Article 100113. https://doi.org/10.1016/j.foostr.2019.100113

Aveyard, R., Binks, B. P., & Clint, J. H. (2003). Emulsions stabilised solely by colloidal particles. *Advances in Colloid and Interface Science, 100–102*, 503–546. https://doi.org/10.1016/S0001-8686(02)00069-6

Bhatluri, K. K., Chakraborty, S., Manna, M. S., Ghoshal, A. K., & Saha, P. (2015). Separation of toxic heavy metals from its aqueous solution using environmentally

benign vegetable oil as liquid membrane. *RSC Advances, 5*(107), 88331–88338. https://doi.org/10.1039/C5RA13260F
Binks, B. P. (2002). Particles as surfactants—Similarities and differences. *Interface Science*.
Binks, B. P., & Lumsdon, S. O. (2000). Influence of particle wettability on the type and stability of surfactant-free emulsions. *Langmuir, 16*(23), 8622–8631. https://doi.org/10.1021/la000189s
Chen, L., Ao, F., Ge, X., & Shen, W. (2020). Food-grade pickering emulsions: Preparation, stabilization and applications. *Molecules, 25*(14), Article 3202. https://doi.org/10.3390/molecules25143202
Chevalier, Y., & Bolzinger, M.-A. (2013). Emulsions stabilized with solid nanoparticles: Pickering emulsions. *Colloids and Surfaces A: Physicochemical and Engineering Aspects, 439*, 23–34. https://doi.org/10.1016/j.colsurfa.2013.02.054
Chierotti, M. R., Ferrero, L., Garino, N., Gobetto, R., Pellegrino, L., Braga, D., Grepioni, F., & Maini, L. (2010). The richest collection of tautomeric polymorphs: The case of 2-thiobarbituric acid. *Chemistry – A European Journal, 16*(14), 4347–4358. https://doi.org/10.1002/chem.200902485
Coquerel, G. (2014). Crystallization of molecular systems from solution: Phase diagrams, supersaturation and other basic concepts. *Chemical Society Reviews, 43*(7), 2286–2300. https://doi.org/10.1039/C3CS60359H
Dai, Y., Terskikh, V., Brinmkmann, A., & Wu, G. (2020). Solid-state 1H, 13C, and 17O NMR characterization of the two uncommon polymorphs of curcumin. *Crystal Growth & Design, 20*(11), 7484–7491. https://doi.org/10.1021/acs.cgd.0c01164
Desiraju, G. R. (2013). Crystal engineering: From molecule to crystal. *Journal of the American Chemical Society, 135*(27), 9952–9967. https://doi.org/10.1021/ja403264c
Dickinson, E. (2010). Food emulsions and foams: Stabilization by particles. *Current Opinion in Colloid & Interface Science, 15*(1–2), 40–49. https://doi.org/10.1016/j.cocis.2009.11.001
Ewens, H., Metilli, L., & Simone, E. (2021). Analysis of the effect of recent reformulation strategies on the crystallization behaviour of cocoa butter and the structural properties of chocolate. *Current Research in Food Science, 4*, 105–114. https://doi.org/10.1016/j.crfs.2021.02.009
Fisher, L. R., Mitchell, E. E., & Parker, N. S. (1985). Interfacial tensions of commercial vegetable oils with water. *Journal of Food Science, 50*(4), 1201–1202. https://doi.org/10.1111/j.1365-2621.1985.tb13052.x
Frelichowska, J., Bolzinger, M.-A., Pelletier, J., Valour, J.-P., & Chevalier, Y. (2009). Topical delivery of lipophilic drugs from o/w Pickering emulsions. *International Journal of Pharmaceutics, 371*(1–2), 56–63. https://doi.org/10.1016/j.ijpharm.2008.12.017
French, D. J., Taylor, P., Fowler, J., & Clegg, P. S. (2015). Making and breaking bridges in a Pickering emulsion. *Journal of Colloid and Interface Science, 441*, 30–38. https://doi.org/10.1016/j.jcis.2014.11.032
Heffernan, C., Ukrainczyk, M., Zeglinski, J., Hodnett, B. K., & Rasmuson, Å. C. (2018). Influence of Structurally Related Impurities on the Crystal. Nucleation of Curcumin. *Crystal Growth & Design, 18*(8), 4715–4723. https://doi.org/10.1021/acs.cgd.8b00692
Jafari, S. M., Sedaghat Doost, A., Nikbakht Nasrabadi, M., Boostani, S., & Van der Meeren, P. (2020). Phytoparticles for the stabilization of Pickering emulsions in the formulation of novel food colloidal dispersions. *Trends in Food Science & Technology, 98*, 117–128. https://doi.org/10.1016/j.tifs.2020.02.008
Klitou, P., Parisi, E., Bordignon, S., Bravetti, F., Rosbottom, I., Dell'Aera, M., Cuocci, C., Chierotti, M. R., Altomare, A., & Simone, E. (2023). Navigating the complex solid form landscape of the quercetin flavonoid molecule. *Crystal Growth & Design, 23*(8), 6034–6045. https://doi.org/10.1021/acs.cgd.3c00584
Klitou, P., Rosbottom, I., Karde, V., Heng, J. Y. Y., & Simone, E. (2022). Relating crystal structure to surface properties: A study on quercetin solid forms. *Crystal Growth & Design, 22*(10), 6103–6113. https://doi.org/10.1021/acs.cgd.2c00707
Leardi, R. (2009). Experimental design in chemistry: A tutorial. *Analytica Chimica Acta, 652*(1–2), 161–172. https://doi.org/10.1016/j.aca.2009.06.015
Lee, J.-S., Hsu, C.-K., & Jaw, K.-S. (2001). The thermal properties of KClO4 with different particle size. *Thermochimica Acta, 367–368*, 381–385. https://doi.org/10.1016/S0040-6031(00)00691-2
Liu, Y., Niu, S., Lai, W., Yu, T., Ma, Y., Gao, H., Zhao, F., & Ge, Z. (2019). Crystal morphology prediction of energetic materials grown from solution: Insights into the accurate calculation of attachment energies. *CrystEngComm, 21*(33), 4910–4917. https://doi.org/10.1039/C9CE00848A
Luo, Z., Murray, B. S., Yusoff, A., Morgan, M. R. A., Povey, M. J. W., & Day, A. J. (2011). Particle-stabilizing effects of flavonoids at the oil–water interface. *Journal of Agricultural and Food Chemistry, 59*(6), 2636–2645. https://doi.org/10.1021/jf1041855
Macrae, C. F., Bruno, I. J., Chisholm, J. A., Edgington, P. R., McCabe, P., Pidcock, E., Rodriguez-Monge, L., Taylor, R., Streek, J. V. D., & Wood, P. A. (2008). Mercury CSD 2.0—New features for the visualization and investigation of crystal structures. *Journal of Applied Crystallography, 41*(2), 466–470. https://doi.org/10.1107/S0021889807067908
Meenan, P. (2001). From molecules to crystallizers: An introduction to crystallization Roger Davey and John Garside. *Crystal Growth & Design, 1*(1), 101. https://doi.org/10.1021/cg000012w. Oxford University Press, New York. 2000. ISBN 0198504896.
Metilli, L., Storm, M., Marathe, S., Lazidis, A., Marty-Terrade, S., & Simone, E. (2022). Application of X-ray microcomputed tomography for the static and dynamic characterization of the microstructure of oleofoams. *Langmuir, 38*(4), 1638–1650. https://doi.org/10.1021/acs.langmuir.1c03318
Mondal, S., Ghosh, S., & Moulik, S. P. (2016). Stability of curcumin in different solvent and solution media: UV–visible and steady-state fluorescence spectral study. *Journal of Photochemistry and Photobiology B: Biology, 158*, 212–218. https://doi.org/10.1016/j.jphotobiol.2016.03.004
Montis, R., Davey, R. J., Wright, S. E., Woollam, G. R., & Cruz-Cabeza, A. J. (2020). Transforming computed energy landscapes into experimental realities: The role of structural rugosity. *Angewandte Chemie International Edition, 59*(46), 20357–20360. https://doi.org/10.1002/anie.202006939
Nelson, K. M., Dahlin, J. L., Bisson, J., Graham, J., Pauli, G. F., & Walters, M. A. (2017). The essential medicinal chemistry of curcumin: miniperspective. *Journal of Medicinal Chemistry, 60*(5), 1620–1637. https://doi.org/10.1021/acs.jmedchem.6b00975
Okada, M., Maeda, H., Fujii, S., Nakamura, Y., & Furuzono, T. (2012). Formation of Pickering Emulsions Stabilized via Interaction between Nanoparticles Dispersed in Aqueous Phase and Polymer End Groups Dissolved in Oil Phase. *Langmuir, 28*(25), 9405–9412. https://doi.org/10.1021/la3015964
Pandey, K. U., & Dalvi, S. V. (2019). Understanding stability relationships among three curcumin polymorphs. *Advanced Powder Technology, 30*(2), 266–276. https://doi.org/10.1016/j.apt.2018.11.002
Peram, M. R., Jalalpure, S. S., Joshi, S. A., Palkar, M. B., & Diwan, P. V. (2017). Single robust RP-HPLC analytical method for quantification of curcuminoids in commercial turmeric products, Ayurvedic medicines, and nanovesicular systems. *Journal of Liquid Chromatography & Related Technologies, 40*(10), 487–498. https://doi.org/10.1080/10826076.2017.1329742
Prandini, E., Calì, E., Maloney, A. G. P., Parisi, E., & Simone, E. (2024). Predicting particle quality attributes of organic crystalline materials using Particle Informatics. *Powder Technology, 443*, Article 119927. https://doi.org/10.1016/j.powtec.2024.119927
Prasad, R., Gupta, K. M., Poornachary, S. K., & Dalvi, S. V. (2020). Elucidating the polymorphic behavior of curcumin during antisolvent crystallization: Insights from Raman spectroscopy and molecular modeling. *Crystal Growth & Design, 20*(9), 6008–6023. https://doi.org/10.1021/acs.cgd.0c00728
Preston, J. A., Parisi, E., Murray, B., Tyler, A. I. I., & Simone, E. (2024). Elucidating the polymorphism of xanthone: A crystallization and characterization study. *Crystal Growth & Design, 24*(8), 3256–3268. https://doi.org/10.1021/acs.cgd.3c01506
Priyadarsini, K. I. (2009). Photophysics, photochemistry and photobiology of curcumin: Studies from organic solutions, bio-mimetics and living cells. *Journal of Photochemistry and Photobiology C: Photochemistry Reviews, 10*(2), 81–95. https://doi.org/10.1016/j.jphotochemrev.2009.05.001
Pugh, R. J. (2016). *Bubble and foam chemistry*. Cambridge University Press. doi: 10.1017/CBO9781316106938.
Roelands, C. P. M., Jiang, S., Kitamura, M., ter Horst, J. H., Kramer, H. J. M., & Jansens, P. J. (2006). Antisolvent crystallization of the polymorphs of l-Histidine as a function of supersaturation ratio and of solvent composition. *Crystal Growth & Design, 6*(4), 955–963. https://doi.org/10.1021/cg050529d
Sanphui, P., & Bolla, G. (2018). Curcumin, a biological wonder molecule: A crystal engineering point of view. *Crystal Growth & Design, 18*(9), 5690–5711. https://doi.org/10.1021/acs.cgd.8b00646
Sanphui, P., Goud, N. R., Khandavilli, U. B. R., Bhanoth, S., & Nangia, A. (2011). New polymorphs of curcumin. *Chemical Communications, 47*(17), 5013. https://doi.org/10.1039/c1cc10204d
Sarkar, A., & Dickinson, E. (2020). Sustainable food-grade Pickering emulsions stabilized by plant-based particles. *Current Opinion in Colloid & Interface Science, 49*, 69–81. https://doi.org/10.1016/j.cocis.2020.04.004
Simone, E., & Nagy, Z. K. (2015). A link between the ATR-UV/Vis and Raman spectra of zwitterionic solutions and the polymorphic outcome in cooling crystallization. *CrystEngComm, 17*(34), 6538–6547. https://doi.org/10.1039/C5CE00702J
Simone, E., Zhang, W., & Nagy, Z. K. (2015). Application of process analytical technology-based feedback control strategies to improve purity and size distribution in biopharmaceutical crystallization. *Crystal Growth & Design, 15*(6), 2908–2919. https://doi.org/10.1021/acs.cgd.5b00337
Siudem, P., Szeleszczuk, Ł., Zielińska, A., & Paradowska, K. (2023). 13C CPMAS NMR as an alternative method to verify the quality of dietary supplements containing curcumin. *Molecules, 28*(8), Article 3442. https://doi.org/10.3390/molecules28083442
Supran, M. K., Acton, J. C., Howell, A. J., & Saffle, R. L. (1971). Surface tension of common aqueous and organic phases in food emulsions1. *Journal of Milk and Food Technology, 34*(12), 584–585. https://doi.org/10.4315/0022-2747-34.12.584
Tan, C., & McClements, D. J. (2021). Application of advanced emulsion technology in the food industry: A review and critical evaluation. *Foods, 10*(4), Article 812. https://doi.org/10.3390/foods10040812
Tang, J., Quinlan, P. J., & Tam, K. C. (2015). Stimuli-responsive Pickering emulsions: Recent advances and potential applications. *Soft Matter, 11*(18), 3512–3529. https://doi.org/10.1039/C5SM00247H
ter Horst, J. H., Deij, M. A., & Cains, P. W. (2009). Discovering new co-crystals. *Crystal Growth & Design, 9*(3), 1531–1537. https://doi.org/10.1021/cg801200h
Thorat, A. A., & Dalvi, S. V. (2012). Liquid antisolvent precipitation and stabilization of nanoparticles of poorly water soluble drugs in aqueous suspensions: Recent developments and future perspective. *Chemical Engineering Journal, 181–182*, 1–34. https://doi.org/10.1016/j.cej.2011.12.044
Thorat, A. A., & Dalvi, S. V. (2014). Particle formation pathways and polymorphism of curcumin induced by ultrasound and additives during liquid antisolvent precipitation. *CrystEngComm, 16*(48), 11102–11114. https://doi.org/10.1039/C4CE02021A
Thorat, A. A., & Dalvi, S. V. (2015). Solid-state phase transformations and storage stability of curcumin polymorphs. *Crystal Growth & Design, 15*(4), 1757–1770. https://doi.org/10.1021/cg501814q
Wu, J., & Ma, G. (2016). Recent studies of pickering emulsions: Particles make the difference. *Small, 12*(34), 4633–4648. https://doi.org/10.1002/smll.201600877

Xia, T., Xue, C., & Wei, Z. (2021). Physicochemical characteristics, applications and research trends of edible Pickering emulsions. *Trends in Food Science & Technology, 107*, 1–15. https://doi.org/10.1016/j.tifs.2020.11.019

Xiao, J., Sarker, S. D., & Asakawa, Y. (2021). *Handbook of Dietary Phytochemicals*. Springer Singapore. doi: 10.1007/978-981-15-4148-3.

Yang, Y., Fang, Z., Chen, X., Zhang, W., Xie, Y., Chen, Y., Liu, Z., & Yuan, W. (2017). An overview of pickering emulsions: Solid-particle materials, classification, morphology, and applications. *Frontiers in Pharmacology, 8*, Article 287. https://doi.org/10.3389/fphar.2017.00287

Zembyla, M., Murray, B. S., Radford, S. J., & Sarkar, A. (2019). Water-in-oil Pickering emulsions stabilized by an interfacial complex of water-insoluble polyphenol crystals and protein. *Journal of Colloid and Interface Science, 548*, 88–99. https://doi.org/10.1016/j.jcis.2019.04.010

Zembyla, M., Murray, B. S., & Sarkar, A. (2018). Water-in-oil pickering emulsions stabilized by water-insoluble polyphenol crystals. *Langmuir, 34*(34), 10001–10011. https://doi.org/10.1021/acs.langmuir.8b01438

Zembyla, M., Murray, B. S., & Sarkar, A. (2020). Water-in-oil emulsions stabilized by surfactants, biopolymers and/or particles: A review. *Trends in Food Science & Technology, 104*, 49–59. https://doi.org/10.1016/j.tifs.2020.07.028